ELSEVIER

Contents lists available at ScienceDirect

# **Chemical Geology**

journal homepage: www.elsevier.com/locate/chemgeo





# Multi-stage melting of enriched mantle components along the eastern Gakkel Ridge

Yue Cai <sup>a,\*</sup>, Alexandra Yang Yang <sup>b</sup>, Steven L. Goldstein <sup>a,c</sup>, Charles H. Langmuir <sup>d</sup>, Peter J. Michael <sup>e</sup>, James R. Cochran <sup>a</sup>, Wenfang Zhang <sup>f</sup>, Di Wang <sup>g</sup>, Louise Bolge <sup>a</sup>

- <sup>a</sup> Lamont-Doherty Earth Observatory of Columbia University, 61 Rt. 9W, Palisades, NY 10964, USA
- b State Key Laboratory of Isotope Geochemistry, Guangzhou Institute of Geochemistry, Chinese Academy of Sciences, Guangdong, 510640, China
- E Department of Earth and Environmental Sciences, Columbia University, 61 Rt. 9W, Palisades, NY 10964, USA
- d Department of Earth and Planetary Sciences, Harvard University, 20 Oxford St., Cambridge, MA 02138, USA
- <sup>e</sup> Department of Geosciences, University of Tulsa, 800 South Tucker Drive, Tulsa, OK 74104, USA
- f State Key Laboratory of Lake Science and Environment, Nanjing Institute of Geography and Limnology, Chinese Academy of Sciences, 73 East Beijing Road, Nanjing 210008, China
- § State Key Laboratory for Mineral Deposits Research, School of Earth Sciences and Engineering, Nanjing University, 168 Xianlin Avenue, Qixia District, Nanjing 210046, China

#### ARTICLE INFO

Editor: Catherine Chauvel

Keywords:
Mantle melting
Prior melt removal
Enriched mantle
Recycled arc mantle
Mantle metasomatism
High-angle normal faults
Off-axis magmatism

#### ABSTRACT

The global endmember ultra-slow spreading Arctic Gakkel ridge is an ideal place to study mantle melting and the contributions of different mantle components to ridge volcanism. We carried out a high-resolution geochemical study of basalts from a seemingly normal section of the ultraslow-spreading Arctic Gakkel Ridge between 40°E and 60°E, which we refer to as EVZ2. While the majority of volcanics sampled from EVZ2 could be characterized as normal Mid-Ocean Ridge Basalts (NMORB), we identified a group of Isotopically Enriched, Incompatible Element Depleted MORB (IEDMORB) with low MREE/HREE ratios (i.e., "ghost garnet" signature). EVZ2 IED-MORB are mostly found near the rift valley walls away from axial volcanic centers. We propose that IEDMORB are the products of two stages of melting. They are shallow secondary melts of incompatible trace element enriched low-solidus mantle components that had lost some initial melt in the presence of residual garnet at depth. While the deep initial melts are more likely to be focused toward axial volcanic centers and subsequently diluted by normal peridotite melts, some of the shallow secondary melts could erupt as IEDMORB via pre-existing crustal weaknesses, such as deep-rooted high-angle normal faults that are ubiquitous along ultra-slow spreading ridges, thereby preserving their enriched isotopic compositions. While most dredges that sampled IEDMORB also recovered other types of MORB, all the samples from Dredge 55 are IEDMORB with distinctive arc-type trace element signatures, including relative depletion in Nb (and Ta), as well as enrichment in Th and fluid mobile elements (e.g., high Th/Nb, La/Nb, Pb/Ce, and H<sub>2</sub>O/Ce). These signatures suggest that they sampled recycled metasomatized arc-mantle wedge material. Other EVZ2 IEDMORB also show relative enrichment in fluid mobile elements and depletion in Nb (e.g., high La/Nb), but lack enrichment in Th. As Th has extremely low mobility in aqueous fluids, Th enrichment requires metasomatism involving silicate melts. Thus, we propose that the high Th/Nb, high La/Nb IEDMORB contain silicate-melt metasomatized arc mantle wedge material while the low-Th/ Nb, high La/Nb IEDMORB only contain aqueous-fluid metasomatized arc mantle wedge material. Globally, IEDMORB with ghost garnet signatures are mostly found along ridges near mantle plumes where low-solidus, incompatible element and isotopically enriched mantle components that suffered initial melt loss at depth could be entrained in the upwelling subridge mantle and undergo further melting. However, most near-plume IEDMORB do not show arc-type geochemical signatures. Therefore, the discovery of IEDMORB from 20% of dredges along EVZ2, where most ridge volcanics are NMORB with depleted isotopic compositions, reflects the sporadic distribution of recycled arc mantle wedge material in the Arctic mantle and the prevalence of preexisting crustal conduits, such as high-angle normal faults, along ultra-slow spreading ridges that facilitate melt migration with limited melt pooling and mixing.

E-mail address: cai@ldeo.columbia.edu (Y. Cai).

 $<sup>^{\</sup>star}$  Corresponding author.

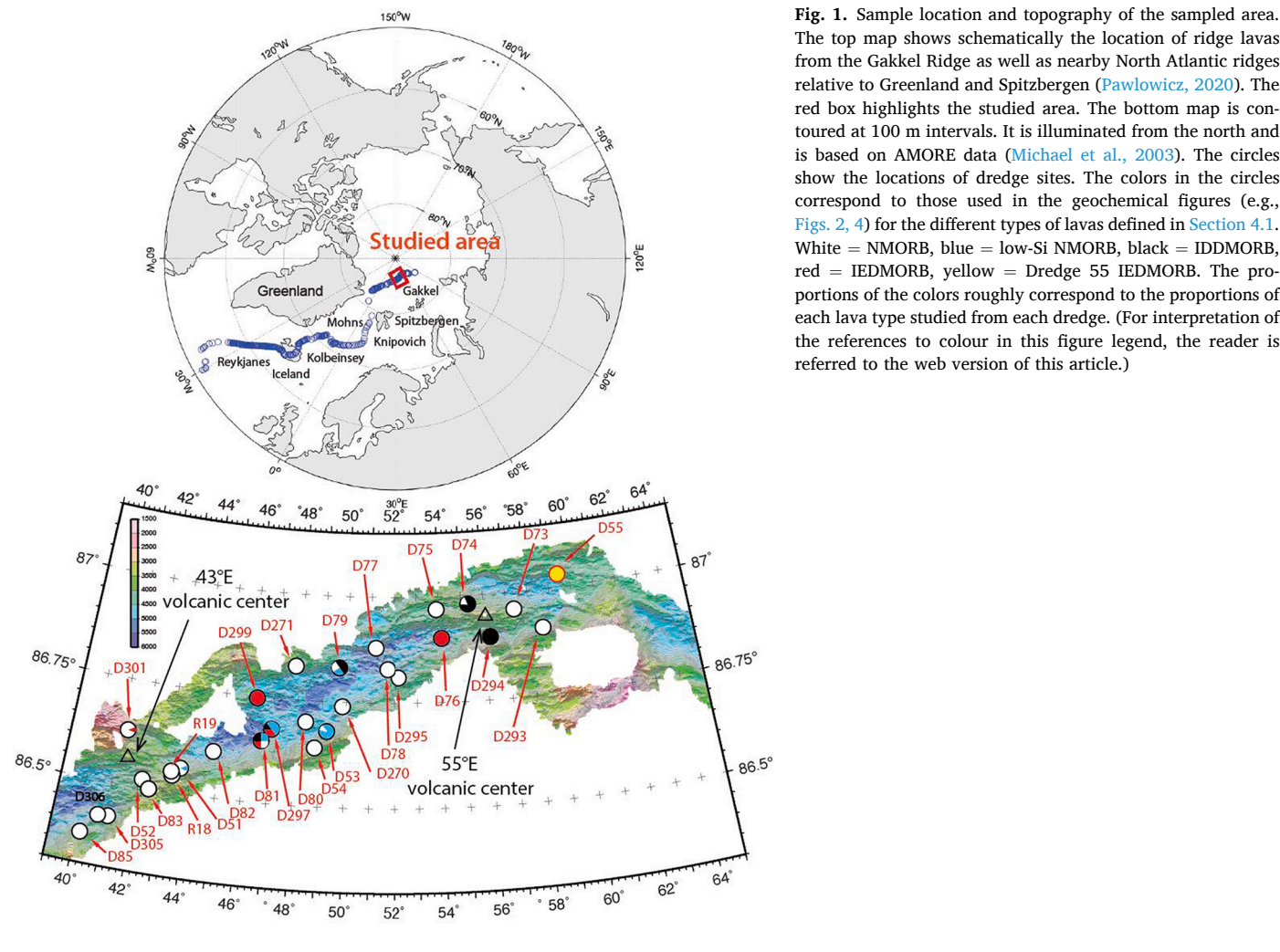
#### 1. Introduction

Ocean ridge volcanics are generally considered as chemically more homogeneous than magmas from other tectonic settings. Nevertheless, it has been well-known for decades that global-scale chemical variations exist within and between ridge segments (e.g., Hofmann and White, 1982; Zindler and Hart, 1986; Rehkämper and Hofmann, 1997; Donnelly et al., 2004; Hémond et al., 2006; Gale et al., 2013; Lambart et al., 2019). Some of the elemental heterogeneities observed in mid-ocean ridge basalts (MORB) could be attributed to shallow-level processes such as fractional crystallization and assimilation of the overlying gabbroic lower oceanic crust (e.g., Lissenberg and Dick, 2008). However, variations in their isotopic compositions require long-term variability of parent/daughter ratios and extended time intervals in the mantle. Within small regions (such as individual ridge segments) parent/daughter ratios and their corresponding isotope ratios often correlate with one another (e.g., Dosso et al., 1999; Donnelly et al., 2004), but this is not always the case (e.g., Yang et al., 2017). Here we present a notable example of such an exception and explore its origin and significance. In this study, "Isotopically enriched" refers to magma compositions with higher Sr. Pb or lower Nd. Hf isotope ratios than the values of average global NMORB (normal mid-ocean ridge basalts) reported by Gale et al. (2013) (i.e.,  $^{143}$ Nd/ $^{144}$ Nd < 0.51308,  $^{87}$ Sr/ $^{86}$ Sr > 0.70281,  $^{206}\text{Pb}/^{204}\text{Pb} > 18.298$ ,  $^{207}\text{Pb}/^{204}\text{Pb} > 15.505$  or  $^{176}\text{Hf}/^{177}\text{Hf} < 10.7028$ 0.283), and "isotopically depleted" refers to those with lower Sr, Pb or higher Nd, Hf isotopic ratios than average NMORB.

Hanson (1977) introduced the concept of melting a "veined mantle"

as an explanation for the observed heterogeneity in basalts, an idea later popularized by Allègre and Turcotte (1986) who likened the mantle to a "marble cake". In this conceptual model, strips of incompatible-element enriched low-solidus components, such as recycled oceanic or continental crust, are dispersed throughout the peridotite mantle matrix and are mixed (inefficiently) through ductile solid state mantle convection. Many processes can generate incompatible element enriched lowsolidus components in the mantle, including recycling of crustal material through subduction (e.g., Zindler and Hart, 1986; Hofmann and White, 1982; Rehkämper and Hofmann, 1997; Hémond et al., 2006; Lambart et al., 2013), delamination of the lower crust (e.g., Lustrino, 2005), and mantle metasomatism from silica-rich and/or volatile-rich fluids (e.g., McKenzie and O'Nions, 1995; Donnelly et al., 2004; Pilet et al., 2008; Dasgupta, 2018). Salters et al. (2011) also attributed segment-scale linear mixing trends observed in Nd—Hf isotope space to mixing of melts from long-lived incompatible element enriched and depleted mantle components. Partial melts from small volumes of longterm enriched or depleted mantle components may lose their elemental and isotopic signatures through dilution by ambient peridotite melts, especially beneath fast-spreading ridges where the extents of mantle melting are high and melt pooling and mixing are prevalent. In contrast, sub-ridge melting and melt mixing are more limited beneath slowspreading ridges, which offer advantages for the study of chemical and isotopic variability in the upper mantle.

The Gakkel Ridge is a global endmember ultraslow-spreading ridge (Coakley and Cochran, 1998; Edwards et al., 2001; Michael et al., 2003; Dick et al., 2003) where there is no evidence for sustained crustal



The top map shows schematically the location of ridge lavas from the Gakkel Ridge as well as nearby North Atlantic ridges relative to Greenland and Spitzbergen (Pawlowicz, 2020). The red box highlights the studied area. The bottom map is contoured at 100 m intervals. It is illuminated from the north and is based on AMORE data (Michael et al., 2003). The circles show the locations of dredge sites. The colors in the circles correspond to those used in the geochemical figures (e.g., Figs. 2, 4) for the different types of lavas defined in Section 4.1. White = NMORB, blue = low-Si NMORB, black = IDDMORB, red = IEDMORB, yellow = Dredge 55 IEDMORB. The proportions of the colors roughly correspond to the proportions of each lava type studied from each dredge. (For interpretation of the references to colour in this figure legend, the reader is referred to the web version of this article.)

magma chambers (Jokat and Schmidt-Aursch, 2007), transform-faults that could offset mantle source continuity, or hotspots along the ridge (Brozena et al., 2003; Cochran et al., 2003; Michael et al., 2003). We carried out a high-density geochemical study of basalts from a section of the Gakkel Ridge between 40°E and 60°E, which we will refer to as EVZ2 ("Eastern volcanic zone sector 2"). The neighboring sections EVZ1 and EVZ3 are affected by additional processes which will be discussed in follow-up papers. The majority of volcanics recovered from EVZ2 fall into the category of NMORB based on the definition of Gale et al. (2013), with primitive mantle normalized La/Sm ratios between 0.8 and 1.5. However, from ~20% of the dredges, we also found lavas with relatively enriched compositions but unusually depleted incompatible element contents. We refer to them as IEDMORB (Isotopically Enriched D-MORB), to distinguish them from the more common Isotopically Depleted D-MORB (IDDMORB). The origins of EVZ2 IEDMORB are the focus of this study. EVZ2 IEDMORB show distinctive "ghost garnet" signatures, which we define as lower MREE/HREE and higher Lu/Hf ratios than average NMORB, in our case,  $(Sm/Yb)_N < 1.15$  and Lu/Hf >0.19 (Fig. 3). Similar to the "ghost plagioclase" signature first proposed by Sobolev et al. (2000), the "ghost garnet" signature is a trace element signature of garnet in magmas that do not contain garnet. At EVZ2, IEDMORB often erupt alongside of NMORB and/or IDDMORB (Fig. 1). We show that EVZ2 IEDMORB are shallow secondary melts of incompatible trace element enriched low-solidus mantle components that had lost some initial melt in the presence of residual garnet at depth.

# 2. The Gakkel Ridge and its Eastern Volcanic Zone 2 (EVZ2)

The Arctic Mid-Ocean Ridge Expedition (AMORE) in 2001 sampled the western  ${\sim}850$  km of the Gakkel Ridge between longitudes  $7^{\circ}W$  to  $86^{\circ}E$  and identified three morphologically distinct sections (Michael et al., 2003): 1) The  ${\sim}200$  km long relatively magmatically robust Western Volcanic Zone (WVZ) from longitudes  $7^{\circ}W$  to  $2^{\circ}E$ , is characterized by a rift valley and linear volcanic axial ridges that rise from the rift valley floor. 2) The  ${\sim}300$  km long Sparsely Magmatic Zone (SMZ), extending from  $2^{\circ}E$  to  $29^{\circ}E$ , is largely amagmatic, with fresh mantle peridotites directly emplaced along the ridge axis. 3) The Eastern Volcanic Zone (EVZ), which extends from  $29^{\circ}E$  to  $85^{\circ}E$ , is characterized by large isolated volcanic centers that are  $50{-}160$  km apart and each extend  $15{-}50$  km along-strike.

The EVZ is characterized by a very deep ( $\sim$ 5000 mbsl) rift valley with limited volcanic activities along most of its length (Cochran, 2008). The full spreading rate along the EVZ is  $\sim$ 10.3 mm/year on average (Vogt et al., 1979; Brozena et al., 2003; DeMets et al., 2010). A series of large volcanic structures are spaced along the rift valley floor at 31°E, 37°E, 43°E, 55°E and 69°E within the well-surveyed portion of the ridge axis while additional volcanic cones protrude above the sediment-filled rift valley to the east (Edwards et al., 2001; Edwards et al., 2010; Michael et al., 2003). The few volcanic cones between the volcanic centers are primarily located at the edges of the rift valley or on ledges of rift valley walls (Cochran, 2008).

Goldstein et al. (2008) reported that Gakkel WVZ basalts have elevated  $^{87}$ Sr,  $^{86}$ Sr, Ba/La and  $^{\Delta8}$ 4Pb values and showed that they form trends in multi-parameter space between normal EVZ Gakkel MORB and alkaline basalts from Spitzbergen/Svalbard that are melts of the Sub-Continental Lithospheric Mantle (SCLM).  $^{\Delta8}$ 4Pb is the difference in  $^{208}$ Pb/ $^{204}$ Pb between the sample and the Northern Hemisphere Reference Line (NHRL) delineated by Pacific and Atlantic MORB (Hart, 1984). Elevated  $^{\Delta8}$ 4Pb is a distinctive signature of Indian Ocean MORB. Goldstein et al. (2008) attributed these chemical signatures in WVZ basalts to the influence of Svalbard SCLM that was delaminated and introduced into the Arctic mantle as the northward propagation of the North Atlantic mid-ocean ridge separated Greenland from Svalbard. Geochemical surveys along the Gakkel Ridge indicated that this SCLM component is only prevalent west of  $^{16}$ E (Goldstein et al., 2008; Cai, 2009), and basalts from Lena Trough just west of the Gakkel Ridge show

an even stronger influence of this SCLM component (Nauret et al., 2011). To avoid potential influences from this SCLM component, this paper focuses on EVZ2, the section between  $40^{\circ}\text{E}$  and  $60^{\circ}\text{E}$ . EVZ2 is also west of  $61^{\circ}\text{E}$ , where the ridge makes a sudden change in strike to the southeast.

Two axial volcanic centers are present along EVZ2 (Fig. 1). The 43°E volcanic center corresponds to an overall shallowing of the entire rift valley floor, whereas the 55°E volcanic center is an elongate volcanic ridge situated within the rift valley that remains relatively deep (Cochran et al., 2003). Abundant magmatic samples were retrieved from dredges between the volcanic centers and near the edge of the rift valley where the overlying oceanic crust is exceedingly thin and the gabbroic layer is largely absent (Jokat and Schmidt-Aursch, 2007). As a result, the extent of mantle melting and magma mixing should be extremely limited away from the volcanic centers. Melt inclusion studies also suggest limited magma pooling and mixing under axial volcanic centers along EVZ2 (Wanless et al., 2014). A summary of dredge locations where DMORB were discovered is provided in the Supplementary Material.

#### 3. Methods

All isotopic and elemental analyses were performed on hand-picked basaltic glasses. Generally, the glass rinds were easily removed from the whole rock using a hammer and a chisel. On rare occasions when a rock saw was used to cut up larger pieces of samples, the sawed surface was polished with alumina sandpaper to remove any metal contaminants. Larger glass chips were gently broken into smaller pieces with a set of high purity steel mortar and pestle. 1–2 mm size glass chips were rinsed and sonicated in DI water and dried at low-temperature prior to microscopic examination where only chips that are free of vesicles and are with minimal surface alteration were selected for chemistry.

# 3.1. Major and trace elements

Major elements were measured using a Cameca SX100 electron microprobe (EMP) at the American Museum of Natural History following routine procedures (e.g., Gale et al., 2011). The unknowns were normalized to JDF-D2 standard and relative 2SD errors for SiO<sub>2</sub>,  $\rm TiO_2$ ,  $\rm Al_2O_3$ , MgO, FeO, and CaO are better than 2%, for K<sub>2</sub>O and Na<sub>2</sub>O are better than 6%, and for MnO and P<sub>2</sub>O<sub>5</sub> are about 10%. Solution trace element data were measured for most samples using a Thermo Xseries Inductively Coupled Mass Spectrometer (ICP-MS) at Harvard University following routine procedures (e.g., Gale et al., 2011) (Table S1). Internal 1RSD for all elements of interest are better than 3%. External reproducibility of VE32 standard is also better than 3% 1RSD for most elements. The measured and normalizing value of VE32 standard and the external reproducibility data are provided in Supplementary Table S1.

Some samples were measured for trace elements using a RESOlution-S155 193 nm Excimer laser connected to a Thermo iCAP Q ICP-MS which is used only for laser ablation analyses at Harvard University. Two points per chip were obtained, and the values reported are the average of the two analyses. Ca content from major element analysis of the same chip was used as an internal standard. Data were then reduced using basalt standard BHVO-2G run in the same run, which was also used as a drift correction standard run every ten analyses. The Harvard lab basalt glass standard VE32 was present in every probe mount, and was analyzed as an unknown with the other samples to get estimates of between run reproducibility over the course of this study (Table S1). VE32 data were very consistent between runs and provide good estimates of the errors in the analyses, which generally scale with concentration.

### 3.2. Water

Concentrations of H<sub>2</sub>O dissolved in glasses were analyzed by Fourier Transform Infrared Spectroscopy (FTIR) at the University of Tulsa using

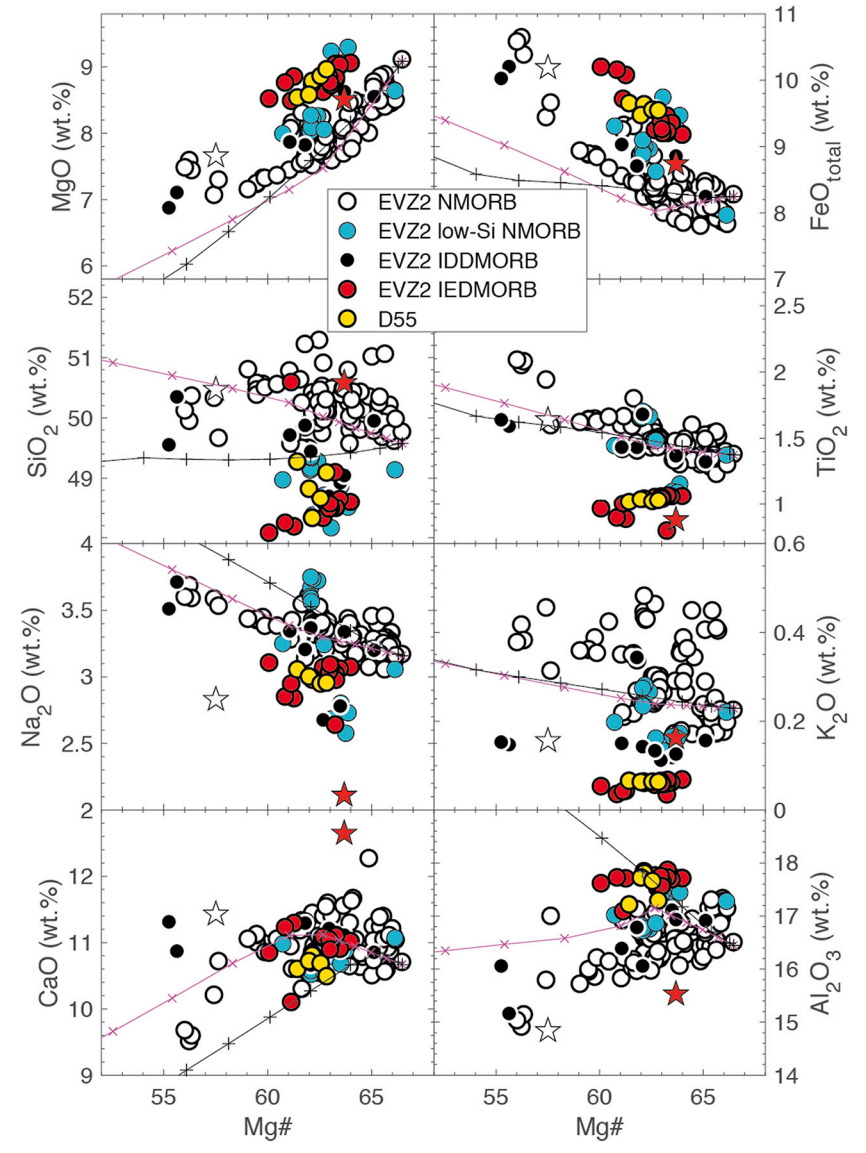


Fig. 2. Major element compositions of EVZ2 basalts in comparison with average global NMORB (white star) (Gale et al., 2013) and average Back-Arc Basin Basalt (BABB, red star) with MgO > 8 wt% calculated from the compilation of Yang et al. (2021). The Liquid Line of Decent (LLD) models are carried out using the Magma Chamber Simulator (Bohrson, 2007) using EVZ2 NMORB D80–9 as the primary melt composition, and assuming a Fe(III)/Fe(II) ratio of 0.15 and 1400  $^{\circ}\text{C}$  as the starting temperature. Purple lines with checker marks represent 1 kbar LLD and black lines with crosses represent 5 kbar LLD. (For interpretation of the references to colour in this figure legend, the reader is referred to the web version of this article.)

published methods and calibrations (Dixon et al., 1988, 1995) with slight modifications (Michael et al., 2003). Doubly polished glass wafers, 100-250 µm thick, were placed atop a 2 mm thick KBr pellet and analyzed using a NicPlan IR microscope equipped with a HgCdTe detector, attached to a Nicolet 520 FTIR. Thickness was measured by two methods: initially by digital micrometer, and then by focusing the calibrated z-axis of the FTIR microscope stage on the glass wafer and on the adjacent KBr disk using reflected light. Optically clear areas of known thickness ( $\pm$  2 µm), 80  $\times$  80 µm, were analyzed with 256 scans/ spot. Absorbance at the broad 3550 cm<sup>-1</sup> (combined OH and H<sub>2</sub>O) and 1630 cm<sup>-1</sup> (molecular H<sub>2</sub>O only) peaks were measured after subtraction of interpolated backgrounds. Density was assumed to be 2.8 g/cm<sup>3</sup>. Molar absorption coefficients used for all glasses were: 63 l/mol-cm for 3550 and 25 l/mol-cm for e1630. Analyses are the average of 3-4 spot determinations of 3550 cm<sup>-1</sup> on two separate wafers. Replicate analyses of different wafers from the same specimen were typically reproducible to  $\pm 5\%$  (1RSD). Repeated measurements of VE32 glass yields 0.276  $\pm$ 0.005 wt% (1 s, n = 12) and ALV 519-4-1 yields 0.176  $\pm$  0.005 wt% (1 s, n = 3).

# 3.3. Isotopes

Sr-Nd-Pb-Hf isotopes were measured on representative samples from each dredge chosen on the basis of elemental compositions using either a VG Sector 54 thermal ionization mass spectrometer (TIMS), or a Neptune Plus MC-ICP-MS at Lamont-Doherty Earth Observatory (LDEO). Chemical separations were performed in better than class 100 conditions within the LDEO-AMNH Clean Chemistry Laboratory, following routine procedures outlined in Goldstein et al. (2008) and Cai et al. (2015). Additional information about the isotopic methods is available in the Supplementary Material. Hf isotope ratios are listed as εHf, the deviation in parts per 10,000 from the "chondritic uniform reservoir" <sup>176</sup>Hf/<sup>177</sup>Hf value of 0.282785 (Bouvier et al., 2008). Nd isotope ratios are listed as ɛNd, the deviation in parts per 10,000 from the "chondritic uniform reservoir" value of  $^{143}$ Nd/ $^{144}$ Nd = 0.512638 (Jacobsen and Wasserburg, 1980). Even though Bouvier et al. (2008) also provided an updated CHUR value for <sup>143</sup>Nd/<sup>144</sup>Nd as 0.512630, We used the older estimate from Jacobsen and Wasserburg (1980) because most geochemical literature references the older value to calculate  $\varepsilon Nd$ . The two values only correspond to a small difference of 0.156 epsilon unit.

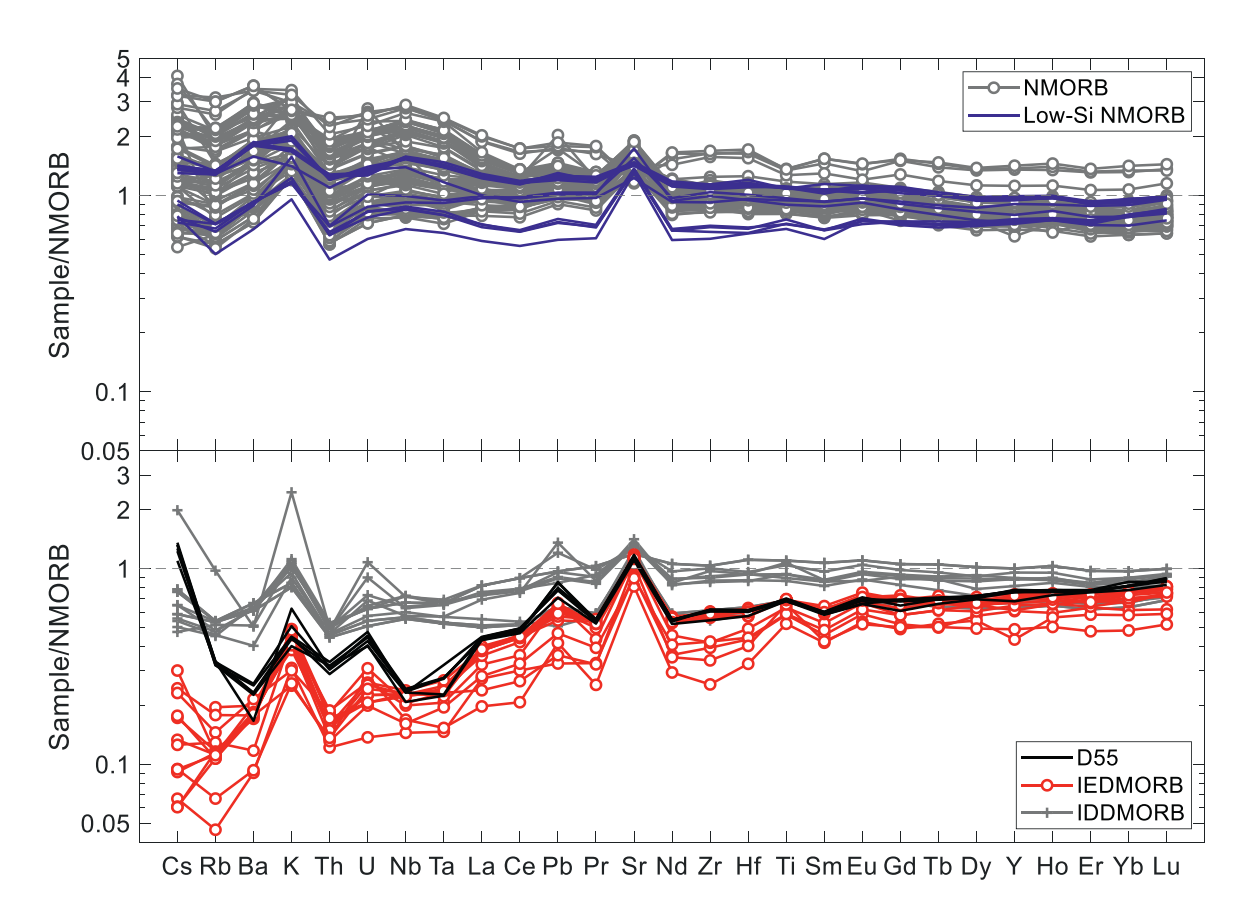


Fig. 3. Spider diagram of different groups of the studied lavas from EVZ2 showing their trace element contents normalized to those of average global NMORB (Gale et al., 2013). Sample 81–131 from the IEDMORB group has an unusually low Cs content of 0.00007 and a N-MORB normalized value of 0.0027. To better illustrate the overall compositional range of the studied lavas, the Cs content of this sample is not plotted.

# 4. Results

We report Sr-Nd-Pb-Hf isotope analyses for  $\sim$ 40 samples from 40°E-60°E along the Gakkel Ridge (EVZ2) in Table S1, along with analyses of major elements and trace elements.

# 4.1. Major and trace element characteristics

Compared with global NMORB, EVZ2 basalts are relatively primitive, with intermediate Mg# [=  $100 \times \text{molar Mg/(Mg} + \text{Fe}$ ), all Fe as  $Fe^{2+}$ ] ranging from 55 to 67, average to low  $SiO_2$  (48.2–50.9 wt%),  $TiO_2$ (0.6-2.2 wt%); and average to high MgO (7.0-8.9 wt%), Al<sub>2</sub>O<sub>3</sub> (15.9-17.9 wt%), and Na<sub>2</sub>O (2.5-3.8 wt%) (Fig. 2). They show a large range of incompatible element contents and ratios, e.g., K<sub>2</sub>O from 0.03 to 0.46 wt%,  $P_2O_5$  from 0.05 to 0.3 wt%,  $(Ba/La)_N$  from 0.15 to 1.08,  $(La/Sm)_N$  from 0.4 to 1.5, and  $(Sm/Yb)_N$  from 0.8 to 1.6. About 70% of basalts from this segment fall within the range of NMORB based on the definition of Gale et al. (2013) with (La/Sm)<sub>N</sub> between 0.8 and 1.5 (Fig. 3). The subscript N denotes normalization to primitive mantlenormalized values with REE concentrations taken from Sun and McDonough (1989). EVZ2 MORB show different extents of K, Cs, Rb and U enrichments (Fig. 3), which could reflect mantle source characteristics or seawater alteration (Staudigel and Hart, 1983; Kelley et al., 2003). Meanwhile, some elements are not affected by seawater alteration (e.g., Th, Nb, Ta) and others are minimally affected (e.g., Sr, Pb, REE) (Staudigel and Hart, 1983; Kelley et al., 2003). We will use elements that are minimally affected by seawater alteration in our discussion of the potential mantle source components of EVZ2 MORB.

The samples can be divided into 5 groups.

- (1) EVZ2 NMORB. These are defined as lavas with (La/Sm)<sub>N</sub> between 0.8 and 1.5. NMORB are found both at axial volcanic centers and from dredges between volcanic centers, with lava flows from axial magma centers containing mostly NMORB. Among studied EVZ2 basalts, NMORB have the highest concentrations of K<sub>2</sub>O (0.16–0.48 wt%), TiO<sub>2</sub> (1.24–1.95 wt%), P<sub>2</sub>O<sub>5</sub> (0.14–0.27 wt%), Zr (96–173 ppm), and the highest overall incompatible element concentrations among EVZ2 MORB. They also have the highest LREE/MREE and MREE/HREE ratios, e.g., (Sm/Yb)<sub>N</sub> between 1.16 and 1.58. Even though samples from this group show a large range of LREE/MREE ratios, they share the same overall trace element pattern.
- (2) **EVZ2 low-Si NMORB.** This is a subgroup of EVZ2 NMORB with  $SiO_2 < 49.5$  wt% at MgO  $\geq 8$  wt%. Compared with other EVZ2 NMORB, EVZ2 Low-Si NMORB have higher  $Al_2O_3$  and  $Na_2O$  at a given MgO content. The low-Si NMORB are mostly from Dredges 53 and 297 (Fig. 1), with a few samples from Dredges 51, 79, 81. Among these, only Dredge 51 sampled lavas are associated with volcanism from the 43°E axial volcanic center while the rest are found away from axial volcanic centers.
- (3) EVZ2 isotopically depleted DMORB, or IDDMORB. These are defined as lavas with  $(\text{La/Sm})_N < 0.8$  and  $\epsilon \text{Nd} > 9$ . They were recovered from Dredges 74, 79, 81, 294, and 297 (Fig. 1). Dredge 74 is from the 55°E axial volcanic center while the rest of the dredges sampled away from axial volcanic centers. Their incompatible elements are systematically more depleted than EVZ2 NMORB with  $K_2O < 0.16$  wt%. Their Nd, Pb, and Hf isotopic ratios are more depleted than average NMORB while their Sr isotopes are similar to average NMORB. Detailed descriptions

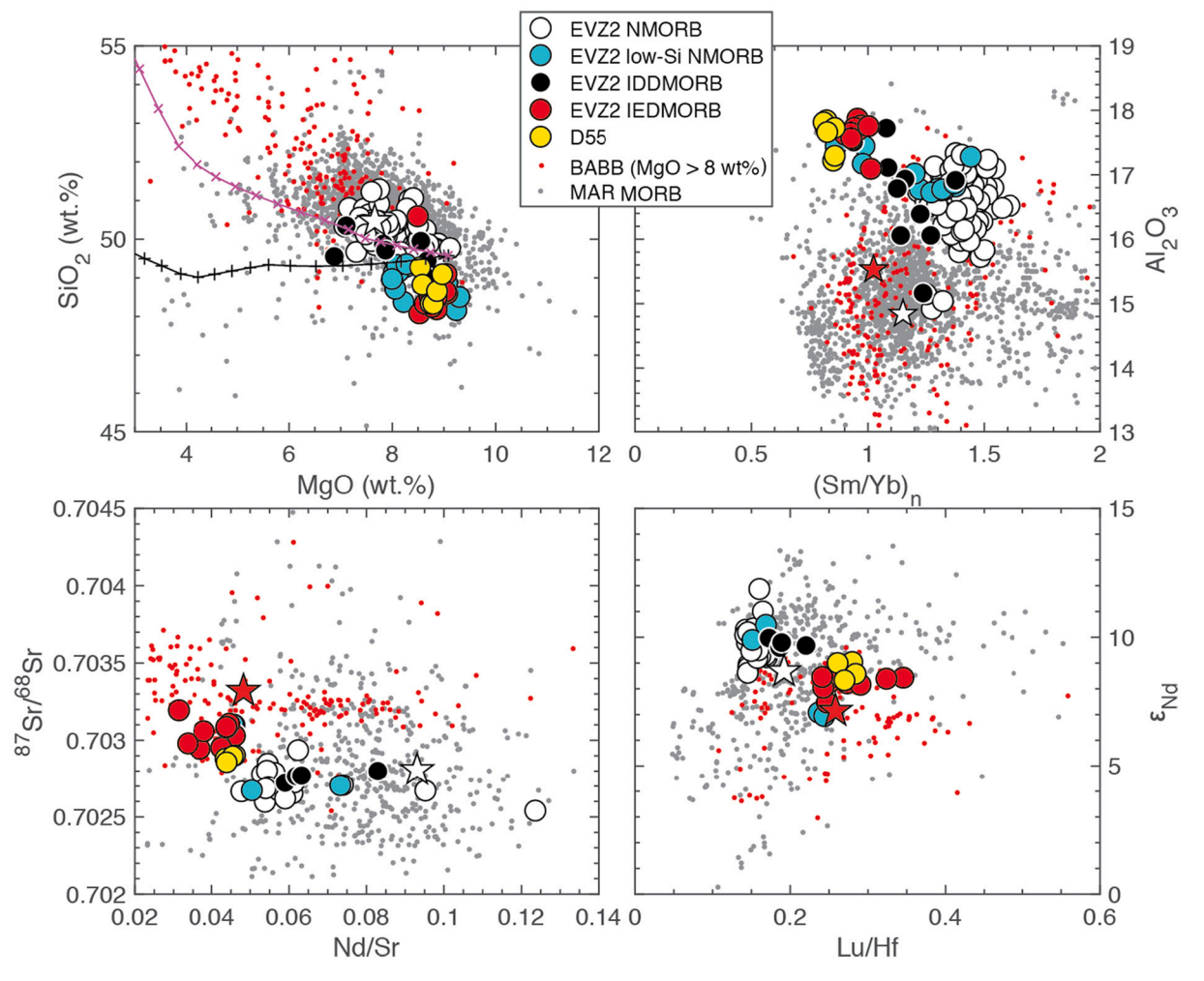


Fig. 4. Major and trace element compositions of the studied samples in a global context with Mid-Atlantic Ridge (MAR) MORB and primitive BABB from Yang et al. (2021). Other symbols follow Fig. 2. In the MgO vs SiO<sub>2</sub> plot, the red star has SiO<sub>2</sub> of 58.6 wt% and MgO of 8.5 wt% which overlaps with one of the IEDMORB and therefore is not shown in the first panel. (For interpretation of the references to colour in this figure legend, the reader is referred to the web version of this article.)

of dredges that recovered DMORB are provided in the Supplementary Information.

- (4) EVZ2 isotopically enriched DMORB, or IEDMORB. These are defined as lavas with  $(\text{La/Sm})_N < 0.8$  and  $\epsilon \text{Nd} < 9$ . EVZ2 IEDMORBs were recovered from Dredges 55, 76, 79, 81, 297, 299 and 301 (Fig. 1), all of which are distant from axial volcanic centers. These samples show "ghost garnet" signatures while most NMORB and IDDMORB from EVZ2 do not (Fig. 3). Despite having the most depleted incompatible elements, these lavas have the most enriched Sr-Nd-Pb-Hf isotopic ratios within EVZ2 (Fig. 5). IEDMORB are found in ~20% of sampled dredges within the study area. Among these dredges, 79, 81 and 301 also encountered NMORB. All IEDMORB show relative depletions of Nb and Ta compared to LREE (i.e., high La/Nb ratios, Fig. 6).
- (5) D55 Samples from Dredge 55 stand out among EVZ2 IEDMORB as the group with the highest Th/Nb, La/Nb and the lowest Ce/Pb ratios along EVZ2 (Fig. 6). They also show the strongest enrichments in Cs, Rb, and U. However, Cs, Rb and U are prone to seawater alteration (e.g., Staudigel and Hart, 1983; Kelley et al., 2003) and thus are not the focus in the following discussions on mantle source components.

# 4.2. Radiogenic isotopes of EVZ2 MORB

EVZ2 samples fall on regional mixing lines that are subparallel to the

NHRL (Northern Hemisphere Reference Line, Hart, 1984) for Pb isotopes. The majority of EVZ2 MORB do not show the type of SCLM signatures recorded by WVZ and Lena Trough lavas, that is, highly radiogenic Sr isotopes (up to 0.7039) and SWIR-type elevated  $^{208}\text{Pb}/^{204}\text{Pb}$  for a given  $^{206}\text{Pb}/^{204}\text{Pb}$  compared to the NHRL, or  $\Delta8/4\text{Pb}$  > 30 (Goldstein et al., 2008; Nauret et al., 2011), except for two samples from the western end of EVZ2: 305-SG3 (NMORB) and 301-SG (IED-MORB) with  $\Delta8/4\text{Pb}$  slightly above 30. This observation indicates that the Greenland-Spitzbergen-type SCLM component is basically absent in EVZ2.

All EVZ2 MORB follow the overall trend delineated by North Atlantic MORB in Pb-Sr-Nd isotope space (Fig. 5). EVZ2 NMORB and IDDMORB occupy the more depleted end of the spectrum while the IEDMORB occupy the more enriched part of the spectrum. There is no evidence that the enriched and depleted mantle components sampled by EVZ2 lavas are drastically different from those sampled by the majority of North Atlantic basalts. However, EVZ2 lavas show lower  $\epsilon$ Hf for a given  $\epsilon$ Nd compared to high latitude North Atlantic ridges, including MORB from Reykjanes Ridge near Iceland (Fig. 5). Blichert-Toft et al. (2005) first discovered that MORB from Mohns and Knipovich ridge plot above the Nd—Hf mantle crust array (Vervoort et al., 2011) with much higher  $\epsilon$ Hf for a given  $\epsilon$ Nd than the mantle crust array (Fig. 5). They attributed this decoupling to disequilibrium melting of subcontinental material. Sanfilippo et al. (2021), on the other hand, attribute this decoupling to remelting of ancient (> 1 Ga) ultra-depleted mantle material caused by

a recent jump in the ridge axis. Regardless of the cause, EVZ2 MORB clearly sampled different mantle components as they fall on the mantle crust array with much lower  $\epsilon Hf$  for a given  $\epsilon Nd$  than Mohns and Knipovich MORB.

#### 5. Discussion

# 5.1. Lower crustal assimilation cannot explain IEDMORB chemistry

Overall, EVZ2 basalts have high Na and Al compared to average NMORB (Fig. 2), which likely resulted from low degrees of mantle melting. EVZ2 NMORB follow 1 kbar low-pressure fractional crystallization trends while EVZ2 IEDMORB do not (Fig. 2). High pressure fractionation could lead to lower magma Si contents and higher Al contents by suppressing plagioclase fractionation (e.g., Eason and Sinton, 2006), however, the major element composition of EVZ2 IEDMORB cannot be reproduced by high pressure fractionation of a primitive EVZ2 NMORB based on the 5 kbar LLD (Figs. 2, 3). Additionally, high pressure fractionation should lead to fractionation of high-Mg clinopyroxene which lowers the Ca and Mg contents of the magmas (Laubier et al., 2012). However, EVZ2 IEDMORB have higher Mg than EVZ2 NMORB. Seawater alteration can also lower Si contents in MORB. However, the decrease in Si contents should be accompanied by a proportional increase in Ti contents (Staudigel and Hart, 1983), which is not observed in EVZ2 IEDMORB or EVZ2 low-Si NMORB (Fig. 2).

Compared to EVZ2 NMORB, EVZ2 IEDMORB have higher Al contents and elevated Sr/Nd ratios (Figs. 2, 4). These signatures are often attributed to assimilation of the lower oceanic crust (e.g., Lissenberg and Dick, 2008; Laubier et al., 2012; Yang et al., 2017). For example, Yang et al. (2017) discovered isotopically enriched NMORB with ghost garnet signature, high Al, and low Si near the Crozet plume along the South West Indian Ridge (SWIR) (Fig. 10). Similarly, Laubier et al. (2012) and Gale et al. (2013) discovered IEDMORB with similar characteristics near the Azores. Both studies attributed the high Al and low Si to stronger lower-crustal assimilation associated with thicker lower oceanic crust. However, the oceanic crust along the EVZ is unusually thin (2.6–3.3 km) (Jokat and Schmidt-Aursch, 2007), which makes it unlikely for lower-crustal assimilation to be an important process along EVZ2.

Yang et al. (2019) carried out melt-troctolite interaction experiments and found that closer to the troctolite interface the melt composition shifted to lower Si, Fe, and alkalis, but higher Mg and Al and, which is consistent with net consumption of plagioclase and olivine during melt-troctolite interaction. EVZ2 IEDMORB have higher Fe for a given Mg# compared to EVZ2 NMORB (Fig. 2), which cannot be explained by more intensive lower crustal assimilation. Assimilation during fractional crystallization modeling also predicts a decrease in Ca that should be proportional to the decrease in Si because olivine is Ca poor (Lissenberg and Dick, 2008). However, EVZ2 IEDMORB have similar Ca contents as EVZ2 NMORB. Higher assimilated plagioclase/olivine ratio could explain the elevated Al contents and Sr/Nd ratios without the accompanying decrease in magma Ca contents. However, this should lead to lower magmatic Mg contents. But EVZ2 IEDMORB have higher Mg than EVZ2 NMORB.

Trace element modeling demonstrates that assimilation of the lower oceanic crust alone cannot generate the observed elemental and isotopic signatures of EVZ2 IEDMORB. Using olivine gabbro (Hart et al., 1999) or troctolite (Godard et al., 2009), one would need to mix 30–40% of high-degree partial melts (e.g., >70%) with EVZ2 NMORB to generate the observed Sm contents of the IEDMORB. Even so, the resulting melt mixture would still have much higher incompatible/compatible element ratios than the IEDMORB (Table S2). Lower crustal assimilation also cannot account for the observed "ghost garnet" signatures (i.e., low MREE/HREE and high Lu/Hf) of EVZ2 IEDMORB or their enriched isotopic signatures. Therefore, while lower-crustal assimilation may have affected the magma composition of EVZ2 MORB, it is not the main process that generated the differences in elemental and isotopic

compositions between EVZ2 NMORB and EVZ2 IEDMORB. Instead, their compositional differences likely originated from different mantle components.

# 5.2. IEDMORB are secondary melts of enriched mantle components

Melts generated from long-term incompatible element depleted mantle should have depleted Sr-Nd-Pb-Hf isotopic ratios, and vice versa. This relationship breaks down for EVZ2 IEDMORB which have enriched isotopes but depleted incompatible elements (Figs. 3, 4). It was shown above that EVZ2 IEDMORB did not acquire their distinctive isotopic or trace element signatures from lower crustal assimilation. A more likely scenario is that EVZ2 IEDMORB are secondary melts of long-term incompatible-element-enriched low-solidus mantle components that had lost some initial melt shortly before the melting event that generated the IEDMORB. Their "ghost garnet" signatures indicate that the prior melt removal likely occurred in the presence of garnet at depth.

Field studies and models have shown that deeper melts are more likely to be focused toward ridge axes or axial volcanic centers (Hebert and Montési, 2010; Gregg et al., 2012; Sparks and Parmentier, 1991). We hypothesize that deep initial melts from enriched, garnet-bearing mantle sources, with high MREE/HREE ratios and enriched isotopic compositions, are preferentially focused toward axial volcanic centers and are subsequently diluted by ambient peridotite melts to form NMORB. Meanwhile, the solid residue continues to upwell and melt to generate the IEDMORB, some of which could largely escape melt mixing and dilution from ambient peridotite melts and thus preserve their enriched isotopes and "ghost garnet" trace element signatures by erupting through pre-existing crustal weaknesses, such as deep-rooted, high-angle normal faults that are ubiquitous along ultra-slow spreading ridges (e.g., Buck et al., 2005; Tucholke et al., 2008; Sauter et al., 2013).

Seismic studies suggest that high-angle detachment faults at slowspreading ridge axes can extend to over 7 km in depth and intercept the melt zone (e.g., deMartin et al., 2007). Numerical modeling studies also suggest that such large detachment faults should be more prevalent along slower spreading ridges where they can extend well into the melt injection zones and act as conduits for melts to erupt to the surface (Buck et al., 2005; Tucholke et al., 2008; Sauter et al., 2013). This mechanism was called upon to explain the occurrence of abnormally young off-axis lavas (Standish and Sims, 2010) and highly focused volcanic features from amagmatic segments along the ultraslow spreading SWIR (Sauter et al., 2004). Cochran (2008) also observed that the seamounts between volcanic centers along the EVZ were likely fed by magmas that ascended along faults as they are primarily situated at the edges of the rift valley. All EVZ2 IEDMORB are found away from volcanic centers and near the edges of the rift valley, some of which are clearly associated with fault structures (detailed descriptions of these dredge locations are provided in the Supplementary Material). These observations support our hypothesis that EVZ2 IEDMORB are shallow secondary melts of isotopically enriched sources in the Gakkel mantle that had previously lost some melt at depth.

# 5.3. Evidence for recycled arc mantle wedge material

Lavas from Dredge 55 have similar major element compositions and MREE/HREE ratios as other EVZ2 IEDMORB. However, their elevated Th/Nb and Pb/Ce ratios approach those of primitive back arc-basin basalts (BABB) (Fig. 6). These characteristics suggest that D55 lavas may contain partial melts from a mantle component that was metasomatized in a subduction zone setting, where fluid mobile and lithophile elements were added to the mantle by silica-rich melts and/or fluids derived from the slab while Nb and Ta were held back in the subducting slab. Despite their overall arc-type incompatible element patterns and elevated  $\rm H_2O/Ce$  and Pb/Ce ratios, D55 lavas have much lower trace element contents and Nb/Zr ratios than most BABB and

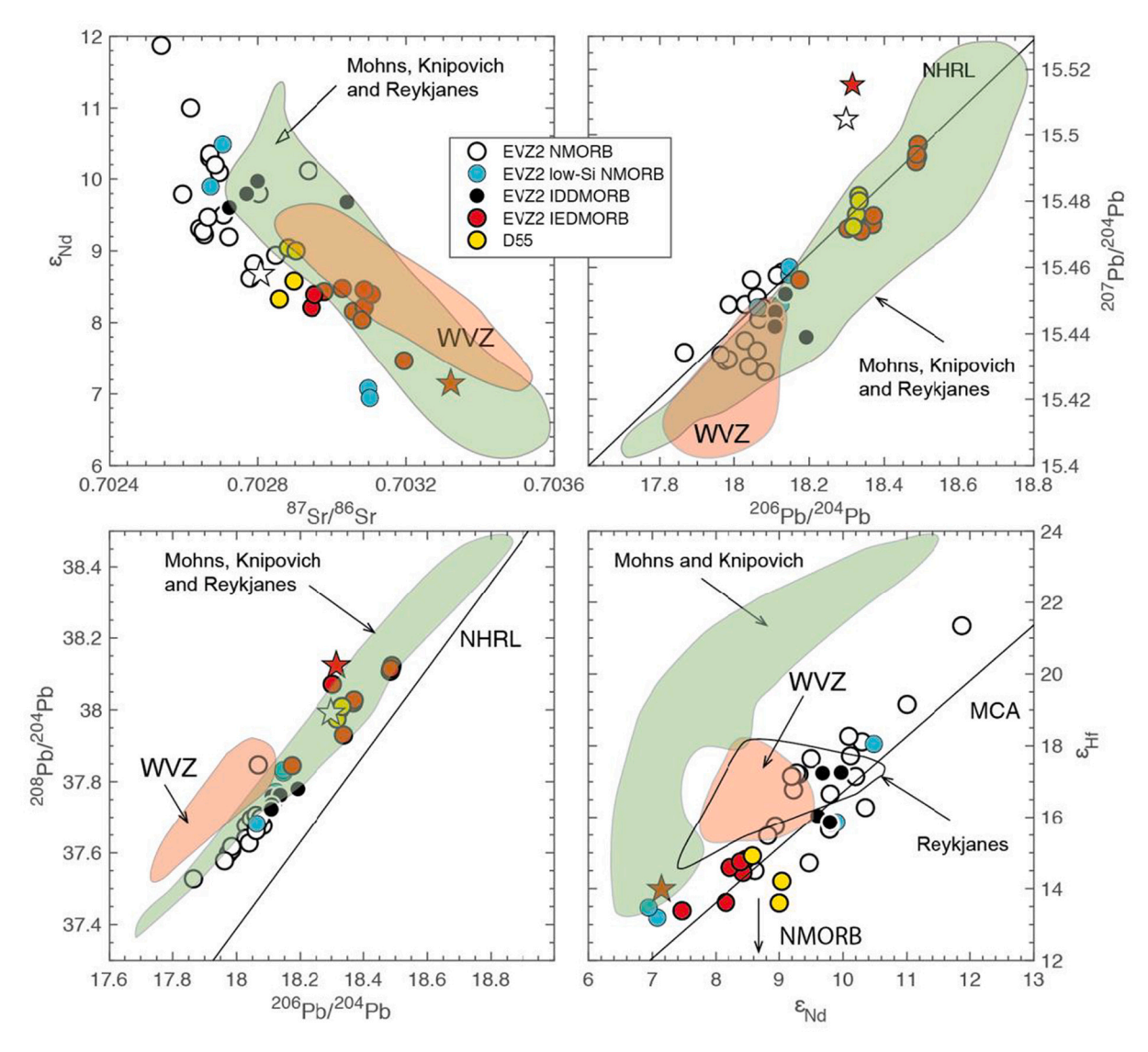


Fig. 5. Isotopic composition of the studied samples in comparison with global MORB (data sources are the same as Fig. 4). Also plotted is the northern hemisphere reference line (NHRL) of Hart (1984) and the mantle-crust array (MCA) of Vervoort et al. (2011). The Gale et al. (2013) average NMORB composition has εHf of 7.6, which is not shown in the figure. Compilation of other high latitude north Atlantic MORB data are from Yang et al. (2021).

MORB. Therefore, D55 lavas are not simple mixtures of melts from peridotites and recycled BABB mantle components. Their depleted trace element contents require additional melt removal from their mantle source along the Gakkel Ridge.

To test this hypothesis, we carried out a modeling exercise. Most BABB have higher <sup>207</sup>Pb/<sup>204</sup>Pb than EVZ2 IEDMORB and north Atlantic MORB, which likely reflect contributions of Pb from U/Pb-enriched crustal material in these BABB mantle source (Fig. 8). However, BABB from Manus Basin overlap almost perfectly with EVZ2 IEDMORB (Sinton, 2003). We used one of these BABB to calculate the mantle component sampled by EVZ2 IEDMORB using the mineral modes from Salters and Stracke (2004) and assuming 20% equilibrium melting (Table S3).

For the prior melt removal model, the choice of Kd's at different pressures is important because Kd's in Cpx generally increase with decreasing pressure, temperature and Cpx Mg#. The relative importance of these factors also changes with regard to ionic radius (Wood and Blundy, 1997; Bédard, 2014). To be consistent and to include as many elements in the model as possible, we used the 2GPa Kd's compiled by Krein et al. (2020) and calculated the high pressure Cpx Kd's based on the 2GPa/3GPa Cpx Kd ratios used by Salters and Stracke (2004). We adjusted this ratio for a few elements to make them more consistent with

elements with similar compatibility (e.g., Yb and Lu) based on empirical observations (Bédard, 2014 and references therein) (Table S3).

Using these Kd's, we were able to reproduce the overall REE pattern of D55 lavas through 7-8% secondary partial melting of a melt-depleted BABB mantle component after 6% initial melt was removed at 3GPa in the garnet stability field while retaining 0.3% of the initial melt in the mantle residue (Table S3, Fig. 7). The exact amount of initial melt removal and secondary melting may well differ in reality. However, this model exercise validates our hypothesis that D55 IEDMORB could be generated largely from secondary melts of a recycled, recently meltdepleted arc mantle component. Retaining small amounts of initial melt in the mantle residue is necessary to reproduce the abundances of highly incompatible element in D55 lavas (i.e., Cs, Rb, Ba). Moreover, mixing this secondary melt with small amounts of NMORB generates an excellent fit for a typical D55 lava (Fig. 7, Table S3). Using these parameters, higher extents of prior melt removal in the garnet stability field would generate higher HREE/MREE ratios but they do not significantly change the Th/Nb ratios of the secondary melt. For example, when the extent of melt removal increases from 2 to 20%, melt Th/Nb ratio decreases from 0.17 to 0.15 while melt Sm/Yb ratio decreases from 0.75 to 0.49. Additionally, prior melt removal does not significantly

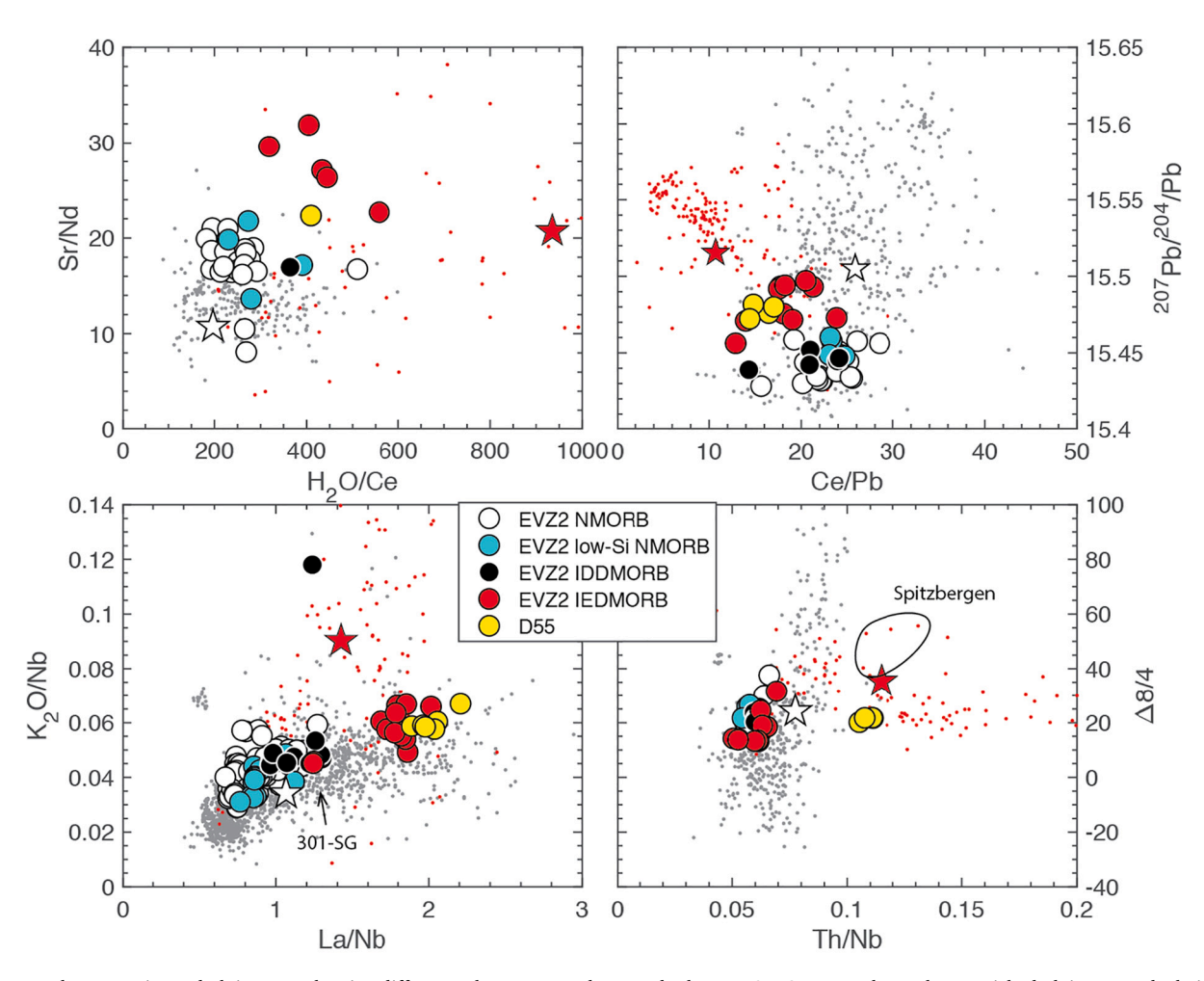


**Fig. 6.** Trace element ratios and Pb isotopes showing differences between D55 lavas and other EVZ2 MORB. D55 lavas show enriched Pb isotopes, depletion in Nb and enrichment in fluid mobile elements (e.g., Sr/Nd, H<sub>2</sub>O/Ce, Pb/Ce). These signatures indicate contribution from arc metasomatized mantle material. The symbols are the same as in Fig. 4.

affect ratios of element pairs with similar compatibilities, such as Ce/Pb, La/Nb and Sr/Nd. Therefore, the elevated Th/Nb, La/Nb, and Sr/Nd in D55 lavas reflect the compositions of their mantle sources rather than the multi-stage melting process. Magma mixing with NMORB, on the other hand, significantly lowers these ratios, which could explain why similar IEDMORB are rarely found along ridges with faster spreading rates which generally correspond to higher extents of partial melting and melt mixing under the ridges.

Finally, to test if EVZ2 NMORB could have sampled some initial melts of the recycled BABB mantle component, we added some deep initial melt from the BABB mantle to a relatively depleted NMORB from EVZ2 (Table S3, Test 4). Addition of this melt would increase the La/Sm and MREE/HREE ratios of the mixture but the mixture would still fall within the observed range of EVZ2 NMORB with up to 30% addition of the deep initial melt (Fig. 7b). EVZ2 NMORB also generally follow the predicted mixing trends (Fig. 9). The primary melts that generated EVZ2 NMORB likely have lower incompatible element abundances to begin with, so EVZ2 NMORB may contain more than 30% of the deep initial melts from a BABB mantle source. These model results, considered together with the moderate enrichment in incompatible elements of EVZ2 NMORB despite their overall more depleted isotopic compositions (Figs. 3, 5), indicate that some EVZ2 NMORB may indeed contain deep initial melts from the recycled BABB mantle source. These findings support our hypothesis that the initial melt of the EVZ2 IEDMORB source are more likely focused toward axial volcanic centers and during this process they would be mixed with ambient peridotite melts.

Addition of deep initial melts to normal peridotite melts would also be an effective way of generating the apparent garnet signature observed in MORB in general (Hirschman and Stolper, 1996).

# 5.4. Do all EVZ2 IEDMORB contain arc mantle component?

D55 lavas and other EVZ2 IEDMORB share similar Pb-Sr-Nd-Hf isotopic ratios, which raises the question: could all EVZ2 IEDMORB be associated with subduction-metasomatized arc mantle? All EVZ2 IEDMORB share similar major element compositions (Fig. 2) as well as trace element ratios that are affected by prior melt removal, such as Nb/Zr and MREE/HREE ratios (Figs. 3, 6), which indicate that their mantle sources underwent similar extents of prior melt removal in the garnet stability field under the Gakkel ridge. D55 lavas and other IEDMORB also share some subduction-related trace element signatures such as elevated  $\rm H_2O/Ce$ ,  $\rm Pb/Ce$ ,  $\rm Sr/Nd$ ,  $\rm K_2O/Nb$ , and the relative depletions of Nb and Ta compared to LREE (e.g., high La/Nb) (Fig. 6). The most important difference between these two groups of lavas is in their Th/Nb ratios.

Could different extents of melt retention during prior melt removal generate the differences between D55 IEDMORB and other EVZ2 IEDMORB? This does not appear to be the case (Table S3, Test 2). If no melt is retained in the mantle source, removing 5% partial melt from the inferred BABB mantle in the garnet stability field followed by 7% partial melt in the spinel stability field would still generate melts with elevated Th/Nb, U/Nb, Pb/Ce and Sr/Nd ratios because each pair of elements

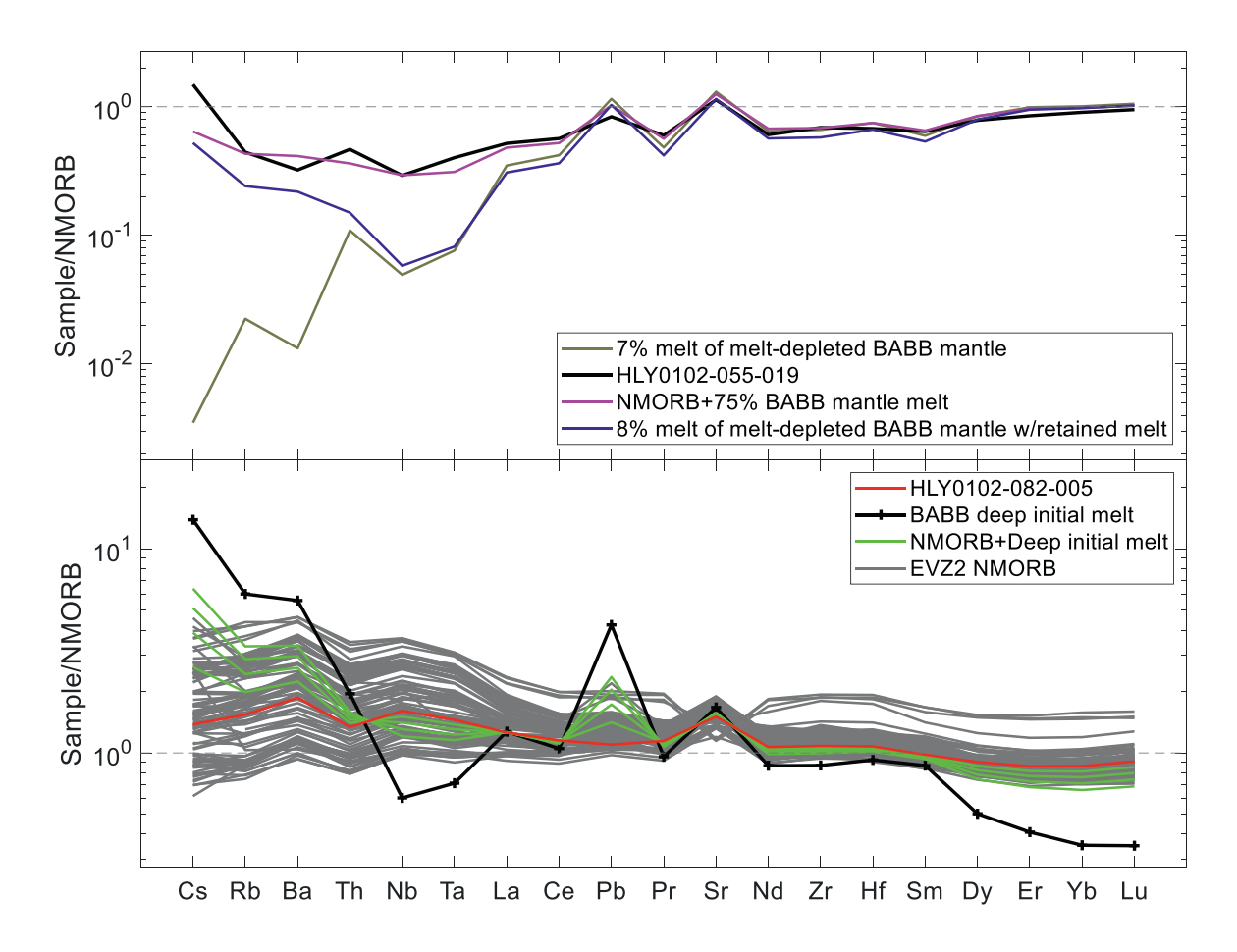


Fig. 7. Prior melt removal modeling results. The top panel shows the excellent match between a typical D55 IEDMORB (D55-19, the black line) and the model result – a 1:3 mixture between NMORB and the modeled secondary melt of a melt-depleted BABB mantle (the purple line). The green lines in the bottom panel represent different mixtures between NMORB and the deep initial melt from the BABB mantle. Addition of up to 30% of the initial melt (the barbed black line) to a typical NMORB (green lines) would still generate a melt composition that falls within the observed range of EVZ2 NMORB (grey lines). Details of the model is presented in Table S3. (For interpretation of the references to colour in this figure legend, the reader is referred to the web version of this article.)

have similar partition coefficients during mantle melting. Therefore, given their distinct Th/Nb ratios, it is clear that the mantle source components that generated most IEDMORB are different from those that generated D55 lavas, even though they all appear to have originated from long-term incompatible element enriched mantle sources with relative depletions of Nb and Ta compared to the LREE.

Instead, we propose that the mantle sources of the EVZ2 IEDMORB with elevated La/Nb but low Th/Nb sampled mantle material that was metasomatized by hydrous fluids rather than silicate melts in a subduction zone setting. In contrast to Pb, Sr, and REE, Th is largely immobile in aqueous fluids (e.g., Nisbet et al., 2018). High Th concentration is a feature of incompatible element enriched continental crust and sediments, but not of the oceanic crust or the depleted mantle. Thus, it is possible that some metasomatized mantle wedge do not have high concentrations of Th, particularly in subduction zones associated with older and colder slabs or arcs starved of sediments. The metasomatized mantle wedge in these arcs may still have elevated La/Nb and Sr/Nb ratios. Although rare, BABB with elevated H<sub>2</sub>O/Ce ratios and MORB-like low Th/Nb ratios have been observed in the Manus Basin (Sinton, 2003), the Marianas (Pearce et al., 2005) and the Lau Basin (e.g., Tian et al., 2011). A mantle component similar to those that generated these BABB could have been sampled by the low Th/Nb, high La/Nb EVZ2 IEDMORB.

It is possible that the mantle source of the low Th/Nb IEDMORB acquired their elevated La/Nb ratios and enriched fluid mobile elements through other kinds of metasomatic processes. However, a few potential

sources could be ruled out: 1) OIB-type deep mantle: as it is well-established that OIB have elevated Ti, Nb and Ta (e.g., Jackson et al., 2008) but EVZ2 IEDMORB have low Nb/La and clear negative Nb anomalies (Figs. 3, 6), and 2) SCLM components with elevated Th/Nb ratios like the kind that was sampled by basalts from Spitzbergen, Lena Trough and the western Gakkel Ridge (Goldstein et al., 2008; Nauret et al., 2011): because these IEDMORB do not have elevated Th/Nb ratios (Fig. 6).

#### 5.5. Petrogenesis of other EVZ2 MORB

EVZ2 NMORB are similar to global NMORB in trace element abundances (Gale et al., 2013). Their higher Na and Ti contents likely reflect overall lower degrees of melting than average global NMORB (Fig. 2). EVZ2 IDDMORB have more enriched incompatible elements than EVZ2 IEDMORB and lack ghost garnet signatures. Their trace element compositions are consistent with their depleted isotopic composition, which suggests "normal" mantle depletion.

Most low-Si NMORB are indistinguishable from EVZ2 NMORB except for two samples: D297-81 and D297-9 (Dredge 297 location is shown in Fig. 1). They have the lowest La/Sm ratios among low-Si NMORB and show enriched Nd and Sr isotope ratios (Figs. 3, 4). These two samples also have ghost garnet signatures (e.g., low Sm/Yb and Dy/Yb). Other samples from the same dredge are IEDMORB. Even though these two samples do not have Nb and Ta depletions like other IEDMORB, they may also have originated from enriched mantle sources that underwent

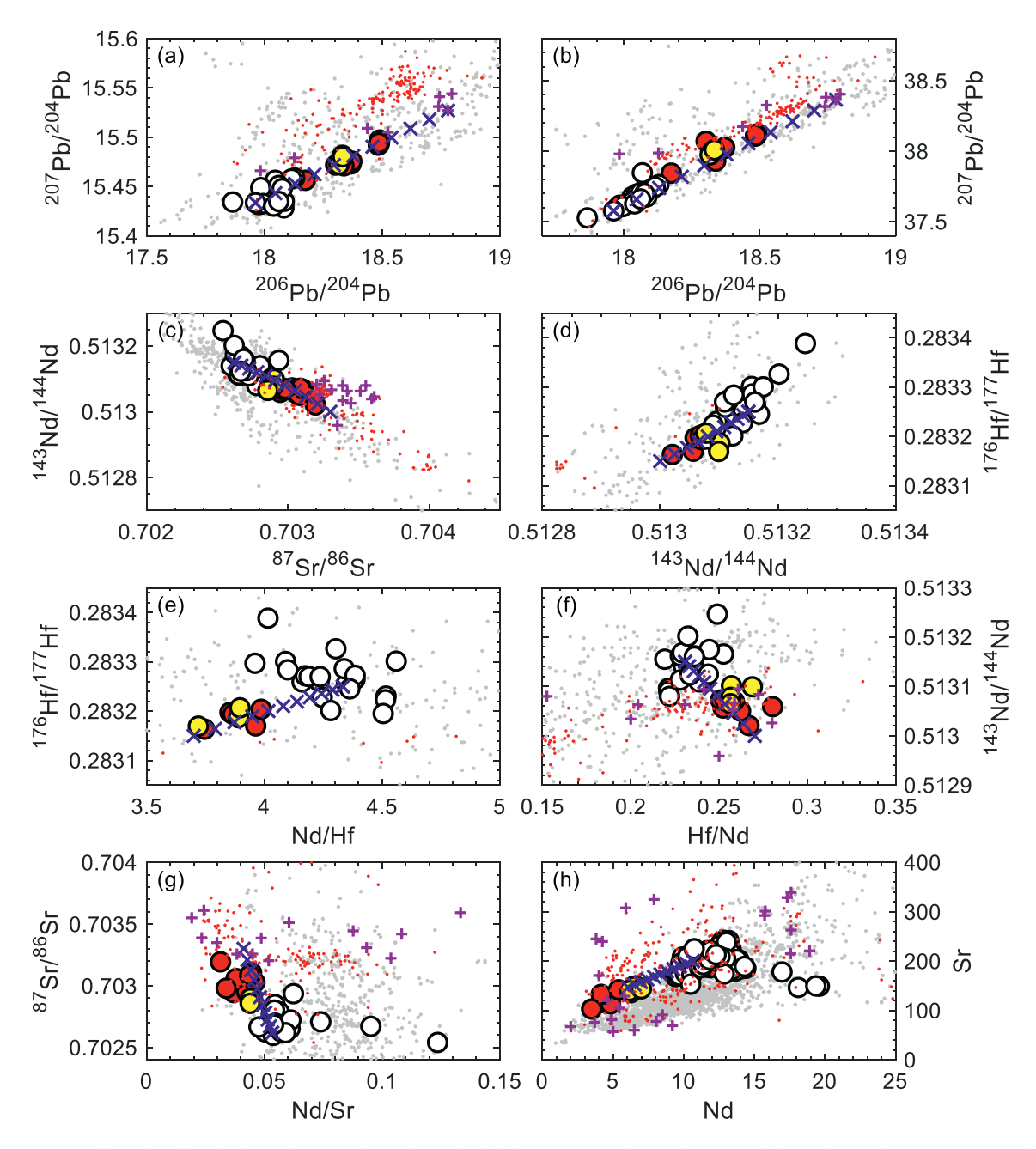


**Fig. 8.** The mixing model results (blue check marks) plotted together with global MORB (grey dots) and BABB (red dots). The purple crosses represent basalts from the Manus basin while the blue check marks delineate the mixing line between NMORB and the secondary melt of a melt-depleted BABB mantle component modeled using a back-arc basalt from the Manus Basin (Sinton, 2003, purple crosses). Other symbols follow the figures above. The model calculation is outlined in Table S3. (For interpretation of the references to colour in this figure legend, the reader is referred to the web version of this article.)

prior melt removal in the garnet stability field. Although they seem to have lost smaller amounts of initial melt than other EVZ2 IEDMORB.

# 5.6. IEDMORB with "ghost garnet" signatures are mostly found near plumes

Prior melt removal may contribute to the elevated Al content in the secondary mantle melts. Hirschmann et al. (2003) generated garnet free melts with high  $Al_2O_3$  (16.2 wt%) at 2GPa and 1400 °C using garnet pyroxenite (Mix1G) as the starting composition. They observed that the melt  $Al_2O_3$  content was lower at higher pressures when garnet was present in the residue, e.g., 14.2 wt% at 2.5 GPa (Hirschmann et al., 2003). Kogiso et al. (2004) melted the same garnet pyroxenite at higher

pressure (5 GPa) and generated melts with much lower  ${\rm Al_2O_3}$  (6.38–10.15 wt%) in the presence of garnet. Based on these results, Kogiso et al. (2004) proposed that garnet effectively holds Al back in the mantle residue during high-pressure melting while the melt Si content is controlled by the bulk Si content of the mantle source.

To test this idea, we screened the global dataset for IEDMORB using the compilation of Yang et al. (2021), which expanded upon the global MORB compilation of Gale et al. (2013). We used the following criteria: (La/Sm) $_N$  < 0.8 and one of the isotopic system that is more "enriched" than the average global NMORB values proposed by Gale et al. (2013), i. e.  $^{143}$ Nd/ $^{144}$ Nd < 0.51308,  $^{87}$ Sr/ $^{86}$ Sr > 0.70281,  $^{206}$ Pb/ $^{204}$ Pb > 18.298,  $^{207}$ Pb/ $^{204}$ Pb > 15.505 or  $^{176}$ Hf/ $^{177}$ Hf < 0.283.

Not including the Gakkel Ridge and the Chile Ridge where

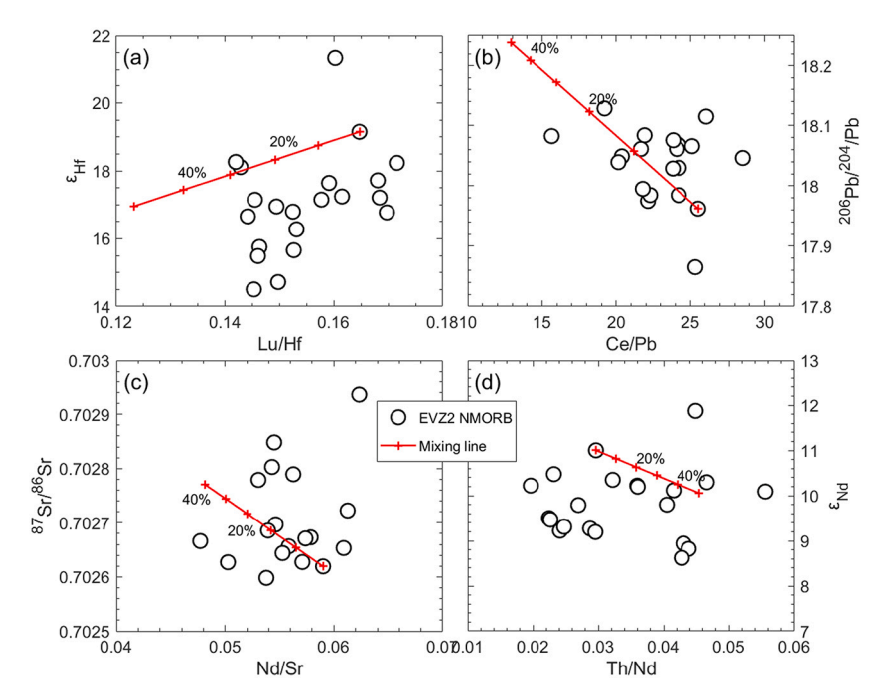


Fig. 9. Mixing model between the deep initial melt of a BABB mantle source and EVZ2 NMORB D82-5 shows that addition of 30% of the initial melt would generate reasonable EVZ2 NMORB compositions. EVZ2 NMORB also follow the mixing trends overall, which supports our hypothesis that some EVZ2 NMORB may contain contributions from deep initial melts of recycled BABB mantle components.

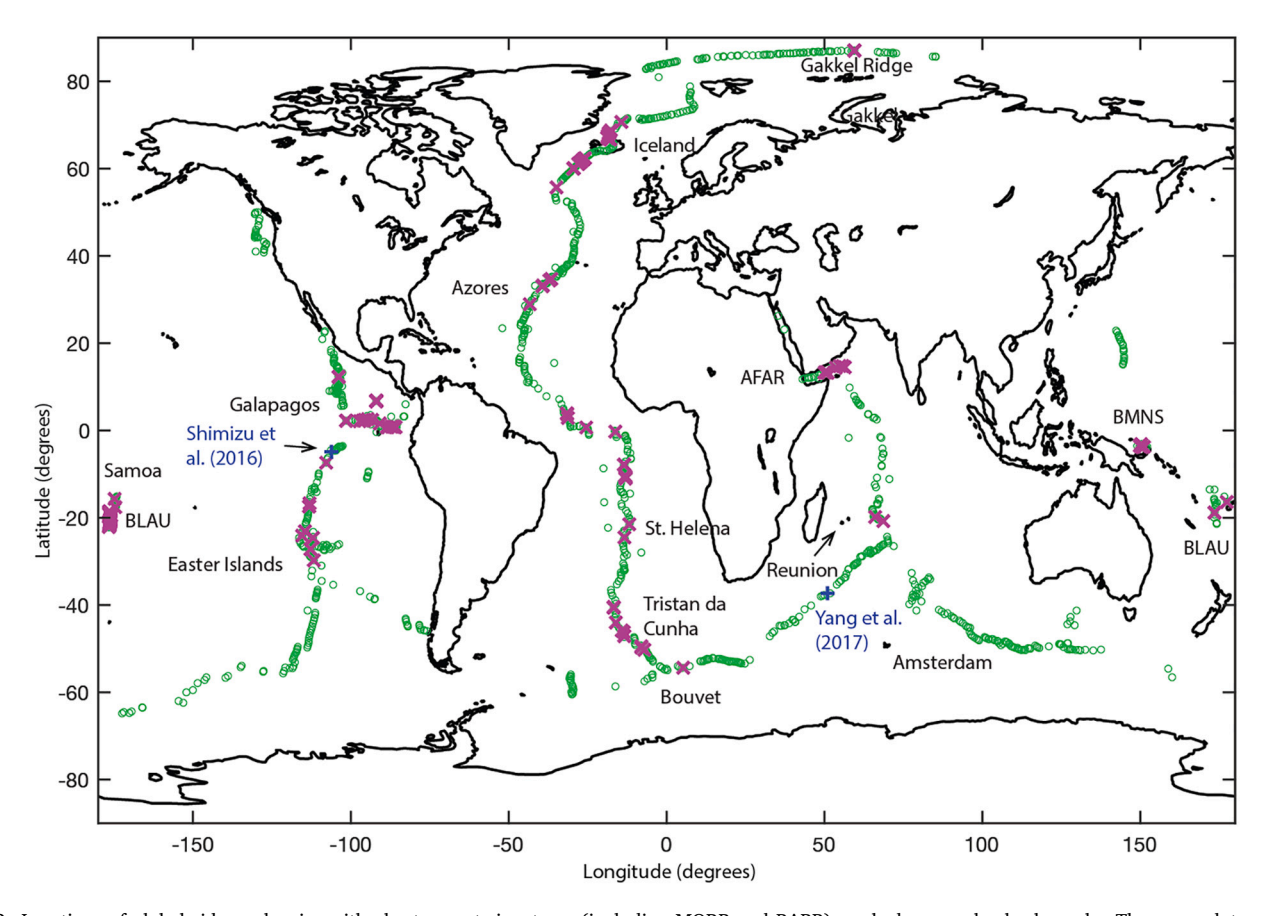


Fig. 10. Locations of global ridge volcanics with ghost garnet signatures (including MORB and BABB) marked as purple check marks. The green dots mark the locations of all the samples included in the dataset from Yang et al. (2021). The locations of samples from Shimizu et al. (2016) and Yang et al. (2017) with similar chemical signatures as EVZ2 IEDMORB are marked with blue crosses. (For interpretation of the references to colour in this figure legend, the reader is referred to the web version of this article.)

subduction modified mantle clearly influences the composition of ridge volcanics, among the 1626 screened MORB with La, Sm, Yb data and at least one isotope ratio of interest, we found 343 IEDMORB (~20%). Among these, 110 ( $\sim$ 7%) have ghost garnet signatures, i.e. (Sm/Yb)<sub>N</sub> < 1. IEDMORB with ghost garnet signatures are mostly found near mantle plumes (Fig. 10). In fact, about half of the samples we identified were reported by Kelley et al. (2013), which focuses on near-plume MORB. Additionally, based on chemistry alone, many BABB would also qualify as IEDMORB with ghost garnet signatures. Overall, global IEDMORB with ghost garnet signature have elevated Mg and Fe and lower Na, Ti and P compared to other MORB, which is consistent with prior melt removal (Fig. S3). However, they do not show elevated Al (Figs. 4, S3). Similarly, Shimizu et al. (2016) discovered a few IEDMORB with modest ghost garnet signatures near the GoFar Fracture Zone along the EPR. They also found no systematic differences in their major element compositions from nearby NMORB. Near-plume IEDMORB also do not show depletion in Nb or enrichment in Th or fluid mobile elements.

These important compositional differences indicate that prior melt removal with residual garnet alone cannot generate the elevated Al contents or the arc-type geochemical signatures of EVZ2 IEDMORB. Instead, these signatures likely originated from the recycled subductionmodified mantle components in the Arctic mantle. Subduction signatures in global MORB are explored more systematically in our companion paper (Yang et al., 2021). However, we make a few relevant observations here. Globally, MORB with high Th/Nb and Pb/Ce ratios are mostly from the Chile Ridge, where arc mantle wedge material made its way into the subridge mantle likely through a nearby slab window (Klein and Karsten, 1995; Bach et al., 1996). Aside from the Chile Ridge and the Gakkel Ridge, only 94 out of 5540 MORB compiled by Yang et al. (2021) have Th/Nb ratios above 0.1, and only 15 of these samples have Pb/Ce ratios above 0.06. Among these samples, only a few from the Kolbeinsey Ridge near Iceland have Th/Nb and Pb/Ce ratios that are comparable with those found in D55 lavas (Andres et al., 2004; Dixon et al., 2017; Blichert-Toft et al., 2005; Kelley et al., 2013). These findings suggest that recycled arc mantle wedge material is prevalent in the high latitude North-Atlantic mantle and the Arctic mantle. As shown in our companion paper (Yang et al., 2021), this is a reasonable conclusion as a number of ancient subduction events could have contributed mantle wedge material to the mantle in this region within the last 200 million years based on plate reconstructions (Seton et al., 2012; Shephard et al.,

There are no hotspots along the Gakkel Ridge. The mantle under the Gakkel Ridge also does not appear fertile overall based on the unusually thin overlying oceanic crust and the predominance of NMORB with relatively depleted Pb-Nd-Hf isotopic ratios. As such, the discovery of IEDMORB with ghost garnet signatures from 20% of dredges throughout EVZ2 likely reflect the sporadic occurrence of enriched components in the Arctic mantle. These enriched components may be fairly common in the upper mantle but their partial melts can be easily diluted through melt pooling and mixing under faster-spreading ridges. Besides high-density sampling, the discovery of these IEDMORB along the Gakkel ridge reflects a combination of low degree partial melting and the abundant pre-existing crustal conduits along this ultra-slow spreading ridge section, such as the high-angle normal faults, which facilitate magma migration with limited mixing and dilution.

# 6. Conclusions

We found isotopically enriched DMORB, or IEDMORB, in the middle of the Eastern Volcanic Zone from the ultra-slow spreading Arctic Gakkel Ridge. We show that they did not acquire their enriched isotopic signatures or depleted trace element patterns from lower crustal assimilation. Instead, we propose that these lavas likely formed as shallow secondary partial melts of incompatible element enriched, garnet-bearing low-solidus mantle components that had lost some initial melt at depth with residual garnet present. While the deeper initial melts

from these enriched components are preferentially focused toward axial volcanic centers, some of their shallower late-stage partial melts could preserve their enriched isotopic signatures by erupting through pre-existing melt conduits such as the high-angle normal faults that are ubiquitous in ultra-slow spreading ridges.

While most dredges that sampled IEDMORB also recovered other types of MORB, all the samples collected from Dredge 55 show distinctive arc-type geochemical signatures, including enriched Th and fluid mobile elements (e.g., high Pb/Ce and  $\rm H_2O/Ce$ ), and depleted high-field strength elements (e.g., high La/Nb and high Th/Nb). These signatures are not significantly affected by the prior melt removal process. We propose that the mantle source of Dredge 55 lavas originated from a mantle sliver that was metasomatized by slab derived silica-rich fluids in a subduction-modified mantle wedge. Other EVZ2 IEDMORB also have elevated La/Nb and variably enriched fluid mobile elements but they lack the enrichment in Th. We propose that these high La/Nb, low Th/Nb EVZ2 IEDMORB may have sampled subduction-modified mantle material that were only metasomatized by aqueous fluids, in subduction zone settings associated with relatively cold slabs.

Globally, IEDMORB with ghost garnet signatures are mostly found near mantle plumes. In such localities their mantle source may have lost some initial melt deep in the melting column due to elevated mantle temperature and plume driven upwelling. While they show similar enriched isotopic compositions and low incompatible element contents as EVZ2 IEDMORB, they lack the arc-type geochemical signatures observed in EVZ2 IEDMORB. This suggests that some of the unique features of EVZ2 IEDMORB, such as the high Al contents, may have been acquired from their mantle source rather than been caused by the multistage melting process.

The majority of magmas from EVZ2 have depleted isotopic compositions with typical NMORB-type elemental compositions. Modeling shows that addition of 30% of initial melts from the IEDMORB source can still generate compositions that are within the observed EVZ2 NMORB spectrum. Given these findings and the fairly even distribution of IEDMORB along the studied ridge segment, it is reasonable to assume that enriched mantle components are fairly common and could be sporadically distributed throughout the upper mantle. But their signatures are best preserved when melting and melt pooling are at minimum and pre-existing crustal conduits are present near the ridge to facilitate melt migration.

#### **Declaration of Competing Interest**

The authors declare that they have no known competing financial interests or personal relationships that could have appeared to influence the work reported in this paper.

# Acknowledgements

We would like to thank Vincent Salters and an anonymous reviewer for detailed and constructive review of the manuscript. Very special thanks are due to the Editor-in-Chief Catherine Chauvel for a very thorough review of the manuscript. We would also like to thank Albrecht Hofmann and Sarah Lambart for valuable feedback; Henry Dick and James Broda for assistance in curating and distributing some of the samples used for this study at WHOI, and Zhongxin Chen for assistance in trace element analysis at Harvard University. This study was partly supported by the Storke Endowment of the Department of Earth and Environmental Sciences, Columbia University and NSF grants 1457293 and 1714892 to YC, 0000389 to CHL and SLG, 0425686 to SLG, and 0425785 to CHL.

# Appendix A. Supplementary data

Supplementary data to this article can be found online at https://doi. org/10.1016/j.chemgeo.2021.120594.

#### References

- Allègre, C.J., Turcotte, D.L., 1986. Implications of a two-component marble-cake mantle.

  Nature 323, 123–127
- Andres, M., Blichert-Toft, J., Schilling, J.G., 2004. Nature of the depleted upper mantle beneath the Atlantic: evidence from Hf isotopes in normal mid-ocean ridge basalts from 79 degrees N to 55 degrees S. Earth Planet. Sci. Lett. 225, 89–103. https://doi. org/10.1016/j.espl.2004.05.041.
- Bach, W., Erzinger, J., Dosso, L., Bollinger, C., Bougault, H., Etoubleau, J., Sauerwein, J., 1996. Unusually large NbTa depletions in North Chile ridge basalts at 36°50′ to 38°56′S: major element, trace element, and isotopic data. Earth Planet. Sci. Lett. 142. 223–240. https://doi.org/10.1016/0012-821X/96100095-7.
- Bédard, J.H., 2014. Parameterizations of calcic clinopyroxene-Melt trace element partition coefficients: CPX partitioning. Geochem. Geophys. Geosyst. 15, 303–336. https://doi.org/10.1002/2013GC005112.
- Blichert-Toft, J., Agranier, A., Andres, M., Kingsley, R., Schilling, J.-G., Albarède, F., 2005. Geochemical segmentation of the Mid-Atlantic Ridge north of Iceland and ridge-hot spot interaction in the North Atlantic. Geochem. Geophys. Geosyst. 6 https://doi.org/10.1029/2004GC000788 n/a-n/a.
- Bohrson, W.A., 2007. Energy-constrained recharge, assimilation, and fractional crystallization (EC-RA(chi)FC): a visual basic computer code for calculating trace element and isotope variations of opensystem magmatic systems. Geochem. Geophys. Geosyst. 8 (11) https://doi.org/10.1029/2007gc001781 doi:Q11003.
- Bouvier, A., Vervoort, J.D., Patchett, P.J., 2008. The Lu-Hf and Sm-Nd isotopic composition of CHUR: constraints from unequilibrated chondrites and implications for the bulk composition of terrestrial planets. Earth Planet. Sci. Lett. 273, 48–57. https://doi.org/10.1016/j.epsl.2008.06.010.
- Brozena, J.M., Childers, V.A., Lawver, L.A., Gahagan, L.M., Forsberg, R., Faleide, J.I., Eldholm, O., 2003. New aerogeophysical study of the Eurasia Basin and Lomonosov Ridge: implications for basin development. Geology 31, 825. https://doi.org/ 10.1130/G19528.1.
- Buck, W.R., Lavier, L.L., Poliakov, A.N.B., 2005. Modes of faulting at mid-ocean ridges. Nature 434, 719–723. https://doi.org/10.1038/nature03358.
- Cai, Y., 2009. Tracing Upper Mantle Heterogeneities with Radiogenic Isotopes at the Mexican Volcanic Belt and the Arctic Gakkel Ridge. Doctoral Thesis. Columbia University.
- Cai, Y., Rioux, M., Kelemen, P.B., Goldstein, S.L., Bolge, L., Kylander-Clark, A.R.C., 2015. Distinctly different parental magmas for calc-alkaline plutons and tholeitic lavas in the central and eastern Aleutian arc. Earth Planet. Sci. Lett. 431, 119–126. https://doi.org/10.1016/j.epsl.2015.07.058.
- Coakley, B.J., Cochran, J.R., 1998. Gravity evidence of very thin crust at the Gakkel Ridge (Arctic Ocean). Earth Planet. Sci. Lett. 162, 81–95. https://doi.org/10.1016/ s0012-821x(98)00158-7.
- Cochran, J.R., 2008. Seamount volcanism along the Gakkel Ridge, Arctic Ocean. Geophys. J. Int. 174, 1153–1173. https://doi.org/10.1111/j.1365-246X.2008.03860.x.
- Cochran, J.R., Kurras, G.J., Edwards, M.H., Coakley, B.J., 2003. The Gakkel Ridge: bathymetry, gravity anomalies, and crustal accretion at extremely slow spreading rates: THE Gakkel Ridge. J. Geophys. Res. 108 https://doi.org/10.1029/ 2002JB001830.
- Dasgupta, R., 2018. Volatile-bearing partial melts beneath oceans and continents—where, how much, and of what compositions? Am. J. Sci. 318, 141–165. https://doi.org/ 10.2475/01.2018.06.
- deMartin, B.J., Sohn, R.A., Pablo Canales, J., Humphris, S.E., 2007. Kinematics and geometry of active detachment faulting beneath the Trans-Atlantic Geotraverse (TAG) hydrothermal field on the Mid-Atlantic Ridge. Geol 35, 711. https://doi.org/ 10.1130/G23718A.1.
- DeMets, C., Gordon, R.G., Argus, D.F., 2010. Geologically current plate motions. Geophys. J. Int. 181, 1–80. https://doi.org/10.1111/j.1365-246X.2009.04491.x.
- Dick, H.J.B., Lin, J., Schouten, H., 2003. An ultraslow-spreading class of ocean ridge. Nature 426, 405–412. https://doi.org/10.1038/nature02128.
- Dixon, J.E., Bindeman, I.N., Kingsley, R.H., Simons, K.K., Le Roux, P.J., Hajewski, T.R., Swart, P., Langmuir, C.H., Ryan, J.G., Walowski, K.J., Wada, I., Wallace, P.J., 2017. Light stable isotopic compositions of enriched mantle sources: Resolving the dehydration paradox. Geochem. Geophys. Geosyst. 18, 3801–3839. https://doi.org/ 10.1002/2016GC006743.
- Dixon, J.E., Stolper, E., Delaney, J.R., 1988. Infrared spectroscopic measurements of CO2 and H2O in Juan de Fuca Ridge basaltic glasses. Earth Planet. Sci. Lett. 90, 87–104. https://doi.org/10.1016/0012-821X(88)90114-8.
- Dixon, J.E., Stolper, E.M., Holloway, J.R., 1995. An experimental study of water and carbon dioxide solubilities in mid-ocean ridge basaltic liquids. Part I: calibration and solubility models. J. Petrol. 36, 1607–1631.
- Donnelly, K.E., Goldstein, S.L., Langmuir, C.H., Spiegelman, M., 2004. Origin of enriched ocean ridge basalts and implications for mantle dynamics. Earth Planet. Sci. Lett. 226, 347–366. https://doi.org/10.1016/j.epsl.2004.07.019.
- Dosso, L., Bougault, H., Langmuir, C.H., Bollinger, C., Bonnier, O., Etoubleau, J., 1999.

  The age and distribution of mantle heterogeneity along the Mid-Atlantic Ridge (31-41°N). Earth Planet. Sci. Lett. 170, 269–286.
- Eason, D., Sinton, J., 2006. Origin of high-Al N-MORB by fractional crystallization in the upper mantle beneath the Galápagos Spreading Center. Earth Planet. Sci. Lett. 252, 423–436. https://doi.org/10.1016/j.epsl.2006.09.048.
- Edwards, M.H., Kurras, G.J., Tolstoy, M., Bohnenstiehl, D.R., Coakley, B.J., Cochran, J. R., 2001. Evidence of recent volcanic activity on the ultraslow-spreading Gakkel Ridge. Nature 409, 808–812. https://doi.org/10.1038/35057258.

- Edwards, M., Cochran, J.R., Dick, H.J.B., 2010. Evidence of recent, off-axis volcanism on Gakkel Ridge, Arctic Ocean. In: Presented at the AGU Fall Meeting Abstracts (pp. V11A-2229).
- Gale, A., Escrig, S., Gier, E.J., Langmuir, C.H., Goldstein, S.L., 2011. Enriched basalts at segment centers: The Lucky Strike (37 degrees 17 \ N) and Menez Gwen (37 degrees 50 \ N) segments of the Mid-Atlantic Ridge. Geochem. Geophys. Geosyst. 12. 10.1029/2010gc003446.
- Gale, A., Dalton, C.A., Langmuir, C.H., Su, Y., Schilling, J.-G., 2013. The mean composition of ocean ridge basalts. Geochem. Geophys. Geosyst. 14, 489–518. https://doi.org/10.1029/2012GC004334.
- Godard, M., Awaji, S., Hansen, H., Hellebrand, E., Brunelli, D., Johnson, K., Yamasaki, T., Maeda, J., Abratis, M., Christie, D., Kato, Y., Mariet, C., Rosner, M., 2009. Geochemistry of a long in-situ section of intrusive slow-spread oceanic lithosphere: results from IODP Site U1309 (Atlantis Massif, 30°N Mid-Atlantic-Ridge). Earth Planet. Sci. Lett. 279, 110–122. https://doi.org/10.1016/j.epsl.2008.12.034.
- Goldstein, S.L., Soffer, G., Langmuir, C.H., Lehnert, K.A., Graham, D.W., Michael, P.J., 2008. Origin of a "Southern Hemisphere" geochemical signature in the Arctic upper mantle. Nature 453, 89–U5. https://doi.org/10.1038/nature06919.
- Gregg, P., Hebert, L., Montési, L., Katz, R., 2012. Geodynamic models of melt generation and extraction at mid-ocean ridges. Oceanography 25, 78–88. https://doi.org/ 10.5670/oceanog.2012.05.
- Hanson, G.N., 1977. Geochemical evolution of suboceanic mantle. J. Geol. Soc. 134, 235–253. https://doi.org/10.1144/gsjgs.134.2.0235.
- Hart, S.R., 1984. A large-scale isotopic anomaly in the Southern Hemisphere mantle. Nature 309, 753–757. https://doi.org/10.1038/309753a0.
- Hart, S.R., Blusztajn, J., Dick, H.J.B., Meyer, P.S., Muehlenbachs, K., 1999. The fingerprint of seawater circulation in a 500-meter section of ocean crust gabbros. Geochim. Cosmochim. Acta 63, 4059–4080. https://doi.org/10.1016/s0016-7037 (99)00309-9.
- Hebert, L.B., Montési, L.G., 2010. Generation of permeability barriers during melt extraction at mid-ocean ridges. Geochem. Geophys. Geosyst. 11.
- Hémond, C., Hofmann, A.W., Vlastélic, I., Nauret, F., 2006. Origin of MORB enrichment and relative trace element compatibilities along the Mid-Atlantic Ridge between 10° and 24°N. Geochem. Geophys. Geosyst. 7 https://doi.org/10.1029/2006GC001317 n/a-n/a.
- Hirschman, M.M., Stolper, E.M., 1996. A possible role for garnet pyroxenite in the origin of the "garnet signature" in MORB. Contrib. Mineral. Petrol. 124 (2), 185–208.
- Hirschmann, M.M., Kogiso, T., Baker, M.B., Stolper, E.M., 2003. Alkalic magmas generated by partial melting of garnet pyroxenite. Geology 31, 481–484.
- Hofmann, A.W., White, W.M., 1982. Mantle plumes from ancient oceanic crust. Earth Planet. Sci. Lett. 57, 421–436. https://doi.org/10.1016/0012-821x(82)90161-3.
- Jackson, M.G., Hart, S.R., Saal, A.E., Shimizu, N., Kurz, M.D., Blusztajn, J.S., Skovgaard, A.C., 2008. Globally elevated titanium, tantalum, and niobium (TITAN) in ocean island basalts with high 3He/4He. Geochem. Geophys. Geosyst. 9 https://doi.org/10.1029/2007GC001876 n/a-n/a.
- Jacobsen, S.B., Wasserburg, G.J., 1980. Sm-Nd isotopic evolution of Chondrites. Earth Planet. Sci. Lett. 50, 139–155. https://doi.org/10.1016/0012-821x(80)90125-9.
- Jokat, W., Schmidt-Aursch, M.C., 2007. Geophysical characteristics of the ultraslow spreading Gakkel Ridge, Arctic Ocean. Geophys. J. Int. 168, 983–998. https://doi. org/10.1111/j.1365-246X.2006.03278.x.
- Kelley, K.A., Plank, T., Ludden, J., Staudigel, H., 2003. Composition of altered oceanic crust at ODP Sites 801 and 1149. Geochem. Geophys. Geosyst. 4 https://doi.org/ 10.1029/2002gc000435.
- Kelley, K.A., Kingsley, R., Schilling, J.G., 2013. Composition of plume-influenced midocean ridge lavas and glasses from the Mid-Atlantic Ridge, East Pacific Rise, Galapagos Spreading Center, and Gulf of Aden. Geochem. Geophys. Geosyst. 14, 223–242. https://doi.org/10.1029/2012gc004415.
- Klein, E.M., Karsten, J.L., 1995. Ocean-ridge basalts with convergent-margin geochemical affinities from the Chile Ridge. Nature 374, 52–57. https://doi.org/ 10.1038/374052a0.
- Kogiso, T., Hirschmann, M.M., Pertermann, M., 2004. High-pressure partial melting of mafic lithologies in the mantle. J. Petrol. 45, 2407–2422. https://doi.org/10.1093/ petrology/egh057.
- Krein, S.B., Behn, M.D., Grove, T.L., 2020. Origins of major element, trace element, and isotope garnet signatures in mid-ocean ridge basalts. J. Geophys. Res. Solid Earth 125. https://doi.org/10.1029/2020JB019612.
- Lambart, S., Laporte, D., Schiano, P., 2013. Markers of the pyroxenite contribution in the major-element compositions of oceanic basalts: review of the experimental constraints. Lithos 160–161, 14–36. https://doi.org/10.1016/j.lithos.2012.11.018.
- Lambart, S., Koornneef, J.M., Millet, M.-A., Davies, G.R., Cook, M., Lissenberg, C.J., 2019. Highly heterogeneous depleted mantle recorded in the lower oceanic crust. Nat. Geosci. 12, 482–486. https://doi.org/10.1038/s41561-019-0368-9.
- Laubier, M., Gale, A., Langmuir, C.H., 2012. Melting and crustal processes at the FAMOUS Segment (Mid-Atlantic ridge): new insights from olivine-hosted melt inclusions from multiple samples. J. Petrol. 53, 665–698. https://doi.org/10.1093/ petrology/epr075
- Lissenberg, C.J., Dick, H.J.B., 2008. Melt–rock reaction in the lower oceanic crust and its implications for the genesis of mid-ocean ridge basalt. Earth Planet. Sci. Lett. 271, 311–325. https://doi.org/10.1016/j.epsl.2008.04.023.
- Lustrino, M., 2005. How the delamination and detachment of lower crust can influence basaltic magmatism. Earth Sci. Rev. 72, 21–38. https://doi.org/10.1016/j. earscirev.2005.03.004.
- McKenzie, D., O'Nions, R.K., 1995. The source regions of ocean island basalts. J. Petrol. 36, 133–159. https://doi.org/10.1093/petrology/36.1.133.
- Michael, P.J., Langmuir, C.H., Dick, H.J.B., Snow, J.E., Goldstein, S.L., Graham, D.W., Lehnert, K., Kurras, G., Jokat, W., Muhe, R., Edmonds, H.N., 2003. Magmatic and

- amagmatic seafloor generation at the ultraslow-spreading Gakkel ridge, Arctic Ocean. Nature 423, 956–U1. https://doi.org/10.1038/nature01704.
- Nauret, F., Snow, J.E., Hellebrand, E., Weis, D., 2011. Geochemical composition of K-rich lavas from the Lena Trough (Arctic Ocean). J. Petrol. 52, 1185–1206. https://doi. org/10.1093/petrology/egr024.
- Nisbet, H., Migdisov, A., Xu, H., Guo, X., van Hinsberg, V., Williams-Jones, A.E., Boukhalfa, H., Roback, R., 2018. An experimental study of the solubility and speciation of thorium in chloride-bearing aqueous solutions at temperatures up to 250 °C. Geochim. Cosmochim. Acta 239, 363–373. https://doi.org/10.1016/j.gca.2018.08.001.
- Pawlowicz, R., 2020. M\_Map: A Mapping Package for MATLAB, Version 1.4m.
- Pearce, J.A., Stern, R.J., Bloomer, S.H., Fryer, P., 2005. Geochemical mapping of the Mariana arc-basin system: Implications for the nature and distribution of subduction components. Geochem. Geophys. Geosyst. 6 https://doi.org/10.1029/ 2004GC000895 n/a-n/a.
- Pilet, S., Baker, M.B., Stolper, E.M., 2008. Metasomatized lithosphere and the origin of alkaline lavas. Science 320, 916–919. https://doi.org/10.1126/science.1156563.
- Rehkämper, M., Hofmann, A.W., 1997. Recycled ocean crust and sediment in Indian Ocean MORB. Earth Planet. Sci. Lett. 147, 93–106. https://doi.org/10.1016/S0012-821X(97)00009-5
- Salters, V.J.M., Stracke, A., 2004. Composition of the depleted mantle. Geochem. Geophys. Geosyst. 5 https://doi.org/10.1029/2003GC000597.
- Salters, V.J.M., Mallick, S., Hart, S.R., Langmuir, C.E., Stracke, A., 2011. Domains of depleted mantle: new evidence from hafnium and neodymium isotopes. Geochem. Geophys. Geosyst. 12, Q08001 https://doi.org/10.1029/2011gc003617.
- Sanfilippo, A., Salters, V.J.M., Sokolov, S.Y., Peyve, A.A., Stracke, A., 2021. Ancient refractory asthenosphere revealed by mantle re-melting at the Arctic Mid Atlantic Ridge. Earth Planet. Sci. Lett. 566, 116981. https://doi.org/10.1016/j. epsl.2021.116981.
- Sauter, D., Mendel, V., Rommevaux-Jestin, C., Parson, L.M., Fujimoto, H., Mével, C., Cannat, M., Tamaki, K., 2004. Focused magmatism versus amagmatic spreading along the ultra-slow spreading Southwest Indian Ridge: evidence from TOBI side scan sonar imagery: ultra-slow spreading Southwest Indian Ridge. Geochem. Geophys. Geosyst. 5 https://doi.org/10.1029/2004GC000738 n/a-n/a.
- Sauter, D., Cannat, M., Rouméjon, S., Andreani, M., Birot, D., Bronner, A., Brunelli, D., Carlut, J., Delacour, A., Guyader, V., MacLeod, C.J., Manatschal, G., Mendel, V., Ménez, B., Pasini, V., Ruellan, E., Searle, R., 2013. Continuous exhumation of mantle-derived rocks at the Southwest Indian Ridge for 11 million years. Nat. Geosci. 6, 314–320. https://doi.org/10.1038/ngeo1771.
- Seton, M., Müller, R.D., Zahirovic, S., Gaina, C., Torsvik, T., Shephard, G., Talsma, A., Gurnis, M., Turner, M., Maus, S., Chandler, M., 2012. Global continental and ocean basin reconstructions since 200Ma. Earth Sci. Rev. 113, 212–270. https://doi.org/10.1016/j.earscirev.2012.03.002.
- Shephard, G.E., Müller, R.D., Seton, M., 2013. The tectonic evolution of the Arctic since Pangea breakup: integrating constraints from surface geology and geophysics with mantle structure. Earth Sci. Rev. 124, 148–183. https://doi.org/10.1016/j.earscirev.2013.05.012.
- Shimizu, K., Saal, A.E., Myers, C.E., Nagle, A.N., Hauri, E.H., Forsyth, D.W., Kamenetsky, V.S., Niu, Y., 2016. Two-component mantle melting-mixing model for the generation of mid-ocean ridge basalts: implications for the volatile content of the

- Pacific upper mantle. Geochim. Cosmochim. Acta 176, 44–80. https://doi.org/10.1016/j.gca.2015.10.033.
- Sinton, J.M., 2003. Magma genesis and mantle heterogeneity in the Manus Back-Arc Basin, Papua New Guinea. J. Petrol. 44, 159–195. https://doi.org/10.1093/petrology/44.1.159.
- Sobolev, A.V., Hofmann, A.W., Nikogosian, I.K., 2000. Recycled oceanic crust observed in "ghost plagioclase" within the source of Mauna Loa lavas. Nature 404, 986–990. https://doi.org/10.1038/35010098.
- Sparks, D.W., Parmentier, E.M., 1991. Melt extraction from the mantle beneath spreading centers. Earth Planet. Sci. Lett. 105, 368–377. https://doi.org/10.1016/ 0012-821X(91)90178-K.
- Standish, J.J., Sims, K.W.W., 2010. Young off-axis volcanism along the ultraslow-spreading Southwest Indian Ridge. Nat. Geosci. 3, 286–292. https://doi.org/10.1038/ngeo824.
- Staudigel, H., Hart, S.R., 1983. Alteration of basaltic glass mechanisms and significance for the oceanic-crust seawater budget. Geochim. Cosmochim. Acta 47, 337–350. https://doi.org/10.1016/0016-7037(83)90257-0.
- Sun, S.-S., McDonough, W.F., 1989. Chemical and isotopic systematics of oceanic basalts: implications for mantle composition and processes. Geol. Soc. Lond., Spec. Publ. 42, 313–345. https://doi.org/10.1144/GSL.SP.1989.042.01.19.
- Tian, L., Castillo, P.R., Hilton, D.R., Hawkins, J.W., Hanan, B.B., Pietruszka, A.J., 2011. Major and trace element and Sr-Nd isotope signatures of the northern Lau Basin lavas: implications for the composition and dynamics of the back-arc basin mantle. J. Geophys. Res. 116 https://doi.org/10.1029/2011JB008791 n/a-n/a.
- Tucholke, B.E., Behn, M.D., Buck, W.R., Lin, J., 2008. Role of melt supply in oceanic detachment faulting and formation of megamullions. Geology 36, 455–458. https:// doi.org/10.1130/g24639a.1.
- Vervoort, J.D., Plank, T., Prytulak, J., 2011. The Hf-Nd isotopic composition of marine sediments. Geochim. Cosmochim. Acta 75, 5903–5926. https://doi.org/10.1016/j. gca.2011.07.046.
- Vogt, P.R., Taylor, P.T., Kovacs, L.C., Johnson, G.L., 1979. Detailed aeromagnetic investigation of the Arctic Basin. J. Geophys. Res. 84, 1071–1089.
- Wanless, V.D., Behn, M.D., Shaw, A.M., Plank, T., 2014. Variations in melting dynamics and mantle compositions along the Eastern Volcanic Zone of the Gakkel Ridge: insights from olivine-hosted melt inclusions. Contrib. Mineral. Petrol. 167.
- Wood, B.J., Blundy, J.D., 1997. A predictive model for rare earth element partitioning between clinopyroxene and anhydrous silicate melt. Contrib. Mineral. Petrol. 129, 166–181. https://doi.org/10.1007/s004100050330.
- Yang, A.Y., Zhao, T.-P., Zhou, M.-F., Deng, X.-G., 2017. Isotopically enriched N-MORB: a new geochemical signature of off-axis plume-ridge interaction—a case study at 50°28′E, Southwest Indian Ridge. J. Geophys. Res. Solid Earth 122, 191–213. https://doi.org/10.1002/2016JB013284.
- Yang, A.Y., Wang, C., Liang, Y., Lissenberg, C.J., 2019. Reaction between mid-ocean ridge basalt and lower oceanic crust: an experimental study. Geochem. Geophys. Geosyst. 20, 4390–4407. https://doi.org/10.1029/2019GC008368.
- Yang, A.Y., Langmuir, C., Cai, Y., Goldstein, S., Michael, P., Chen, Z., 2021. The Subduction Influence on Ocean Ridge Basalts and Its Significance (preprint). In Review. https://doi.org/10.21203/rs.3.rs-132754/v1.
- Zindler, A., Hart, S., 1986. Chemical geodynamics. Annu. Rev. Earth Planet. Sci. 14, 493–571. https://doi.org/10.1146/annurev.ea.14.050186.002425.